Optimization-based Framework for Stability and Robustness of Bipedal Walking Robots

Justin Z. Tang, BE (Hons 1)

A thesis submitted in fulfillment
of the requirements of the degree of
Doctor of Philosophy

THE UNIVERSITY OF
SYDNEY

Australian Centre for Field Robotics
School of Aerospace, Mechanical and Mechatronic Engineering
The University of Sydney

June 2017

Declaration

I hereby declare that this submission is my own work and that, to the best of my knowledge and belief, it contains no material previously published or written by another person nor material which to a substantial extent has been accepted for the award of any other degree or diploma of the University or other institute of higher learning, except where due acknowledgement has been made in the text.

Justin Z. Tang, BE (Hons 1)

June 2017

Abstract

Justin Z. Tang, BE (Hons 1)
The University of Sydney

Doctor of Philosophy
June 2017

Optimization-based Framework for Stability and Robustness of Bipedal Walking Robots

As robots become more sophisticated and move out of the laboratory, they need to be able to reliably traverse difficult and rugged environments. Legged robots – as inspired by nature – are most suitable for navigating through terrain too rough or irregular for wheels. However, control design and stability analysis is inherently difficult since their dynamics are highly nonlinear, hybrid (mixing continuous dynamics with discrete impact events), and the target motion is a limit cycle (or more complex trajectory), rather than an equilibrium. For such walkers, stability and robustness analysis of even stable walking on flat ground is difficult.

This thesis proposes new theoretical methods to analyse the stability and robustness of periodic walking motions. The methods are implemented as a series of pointwise linear matrix inequalities (LMI), enabling the use of convex optimization tools such as sum-of-squares programming in verifying the stability and robustness of the walker. To ensure computational tractability of the resulting optimization program, construction of a novel reduced coordinate system is proposed and implemented.

To validate theoretic and algorithmic developments in this thesis, a custom-built "Compass gait" walking robot is used to demonstrate the efficacy of the proposed methods. The hardware setup, system identification and walking controller are discussed. Using the proposed analysis tools, the stability property of the hardware walker was successfully verified, which corroborated with the computational results.

Acknowledgements

My deep gratitude naturally goes to my advisor, Ian Manchester, for being a constant source of inspiration throughout my PhD. I am thankful for his patience and his mentoring – especially amidst unforeseen circumstances and negative results. I am also grateful for my auxiliary supervisors Humberto Shiromoto and Stefan Williams, for so generously offering their time and knowledge.

My thanks also goes to the wider ACFR community – especially to Jack, Will, Mounir, Felix and Nathan. Thank you for always making time (often late at night) to discuss ideas and the countless coffee runs. To the International House community which has so enriched my time at Sydney University, I am sincerely grateful for the opportunity to be among such diversity and brilliance.

My sincere appreciation also goes to my professors from my undergraduate institutions, The University of Queensland and U.C. Berkeley, and to my supervisors at CSIRO, John Malos and Jonathon Ralston, for inspiring me to undertake doctoral studies.

I would like to further thank the Australian Government and the University of Sydney for supporting my studies through the Australian Postgraduate Award and the Merit Scholarship.

This thesis would never have been possible if not for the unconditional and unwavering love of my family. I am forever indebted to my mother who was willing to sacrifice everything to ensure I have the best possible upbringing. Thanks also to my father who taught me the value of hard work; inspired me to pursue excellence; and truly believed in me before anyone else did. To my extended family and friends – especially my grandmother and my uncles: Daniel, Sam and Howard – who have so tirelessly supported me through thoughts and prayers, you have been my source of strength in my darkest hours. Last but not least, I thank my girlfriend, Jasmine, for her unyielding love and support.

To my parents

Contents

List of Figures

List of Tables

List of Theorems

Chapter 1

Introduction

1.1 Background

The development of legged robots that realise the stability, efficiency and agility of human walking has been the subject of intense research in recent years [21, 33, 85]. Underactuated 'dynamic walkers' can demonstrate amazing feats of efficiency [7], but control design and stability analysis is inherently difficult since their dynamics are highly nonlinear, hybrid (mixing continuous dynamics with discrete impact events), and the target motion is a limit cycle (or more complex trajectory), rather than an equilibrium [33]. For such walkers, stability and robustness analysis of even stable walking on flat ground is difficult.

Efficient computation of basins of stability or robustness (or more generally forward invariant sets) for dynamic walking robots would be an enabling technology for numerous practical problems. For example, they could be used to evaluate different robot designs [61], and to construct switching feedback controllers with guaranteed stability [32, 80].

This thesis makes contributions in this body of research by proposing new theoretical methods to analyse stability and robustness of periodic walking motion – i.e., nonlinear hybrid limit cycles. Computational implementations using convex optimisation

tools are extensively discussed to demonstrate numerical tractability of the proposed methods. Finally, physical hardware verification on a bipedal walker using the new methods are also implemented and discussed.

1.2 Principal Contributions

The principal contributions of this thesis are:

- We propose an extension of the transverse contraction framework to enable computation of inner estimates of the region of stability for limit cycles of hybrid nonlinear systems. Unlike traditional Lyapunov-based methods, the transverse contraction framework developed in this thesis enables proof of stability without prior knowledge of the exact location of the limit cycle in state space. Further, the framework is implemented as a series of pointwise linear matrix inequalities, enabling the use of convex optimisation tools.

- The proposed contraction framework is further extended to study robustness to parametric uncertainty for hybrid nonlinear limit cycles. Since traditional Lyapunov based methods require knowledge of the exact location of the limit cycle in state space, they are not applicable when the system dynamics are uncertain, as uncertainty will generally change the location of the limit cycle. The new proposed framework overcomes this shortcoming.

- For nonlinear hybrid systems of higher dimensions, we introduce simplified construction of the transverse coordinates system, enabling more efficient computation of stability certificates in the reduced coordinates.

- We provide hardware verification of the resulting regions of stability on a real bipedal walking robot. System identification of the walker was carried out and stability analysis via the methods proposed in this thesis was implemented. Physical experiments with the walker successfully validated the computational results.

1.3 Publications

This thesis includes materials from the following peer-reviewed articles which are published or submitted:

- **J. Z. Tang**, I. R. Manchester. Transverse Contraction Criteria for Stability of Nonlinear Hybrid Limit Cycles. *Proceedings of IEEE Conference on Decision and Control*, 2014. (Published)
- **J. Z. Tang**, A. M. Boudali, I. R. Manchester. Invariant Funnels for Underactuated Dynamic Walking Robots: New Phase Variable and Experimental Validation. *Proceedings of the IEEE International Conference on Robotics and Automation (ICRA)*, 2017. (Accepted)
- A. M. Boudali, F. Kong, J. Martinez, **J. Z. Tang**, I. R. Manchester. Design and Modelling of an Open Platform for Dynamic Walking Research. *Proceedings of the IEEE International Conference on Mechatronics*, 2017. (Published)
- **J. Z. Tang**, I. R. Manchester. Transverse Contracting Hybrid Systems and Robust Stability of Dynamic Walking Robots. (Under review)

1.4 Thesis Structure

This thesis proceeds as follows. A literature review covering the current state-of-the-art is presented in Chapter 2. The new transverse contraction analysis framework for hybrid nonlinear systems is presented in Chapter 3. For higher dimensional systems, a simplified construction of the transverse dynamics and the associated reduced coordinate system is presented in Chapter 4. Finally, hardware verification of the proposed method is presented in Chapter 5.

Chapter 2

Literature Review

Stability theory plays a central role in system engineering, especially in the field of control and automation. Stability of a dynamical system, with or without control and disturbance, is a fundamental requirement for its practical value in real-world applications [43]. This is especially true for walking robots, where the control stabilization problem is inherently difficult due the nonlinearity, open-loop instability, hybrid dynamics, and limit-cycle behaviour with target motions which are not necessarily known in advance.

The basic concept of stability emerged as early as 1644 from the study of E. Torricelli, who investigated the equilibrium of a rigid body under the natural force of gravity. In 1788, J. L. Lagrange formulated the classical stability theorem that defines sufficient conditions for stability of equilibrium of any conservative system [59].

Arguably the biggest leap in stability theory was ushered in by the celebrated PhD thesis of A. M. Lyapunov in 1892. Lyapunov's thesis is so fundamental that its basic ideas and techniques are still in use in stability analysis and control of dynamical systems today [18].

In section 2.1, we first discuss the definition and stability analysis of nonlinear limit cycles. Section 2.2 discusses stability analysis of hybrid systems via Lyapunov-based theorems. Then, Section 2.3 introduces recent developments in the notion of contraction theory in stability analysis and its advantages over Lyapunov-based analysis.

An overview of the study of stability and robustness for walking robots is given in Section 2.4. Finally, Section 2.5 outlines the use of semidefinite optimization which provides computationally tractable algorithms for the execution of both Lyapunov and contraction analyses.

2.1 Stability of nonlinear limit cycle

Nonlinear dynamical systems exhibiting oscillating limit cycles are found in a large variety of fields including biology, chemistry, mechanics and electronics [8, 30]. In general, the motion of walking robots can be seen as nonlinear hybrid limit cycles [38, 57]. Studies of limit cycle stability has a long history, dating back to the work of Poincaré in the 19^{th} century.

Consider the dynamics generated by the differential equation:

$$\frac{dx}{dt} = f(x), \quad x \in G \subset \mathbb{R}^n \tag{2.1}$$

where G is closed bounded domain in $\mathbb{R}^n$, f is Lipschitz continuous on G. Further, we denote by $x(t, x_0)$, $0 \leq t < +\infty$, the solution of (2.1) with initial condition $x_0 = x(0, x_0)$

Definition 2.1 (Oscillations)**.** The system in (2.1) *oscillates* when it has a nontrivial periodic solution:

$$x(t + T, x_0) = x(t, x_0), \qquad \forall t \geq 0 \tag{2.2}$$

for some $T > 0$. The minimum T for which (2.2) is true is called the *period*. A set $\mathcal{O} \subset G$ is a *periodic orbit* of (2.1) if

$$\mathcal{O} = \{x \in G : x = x(t, x_0), t \in \mathbb{R}\} \tag{2.3}$$

for some periodic solution $x(t, x_0)$ of (2.2).

Definition 2.2 (Limit Cycles)**.** A *limit cycle* of the system (2.1) is a closed curve

$\Gamma \subset \mathbb{R}^n$ such that Γ is the limit set (or ω-limit set) of the periodic orbit $\mathcal{O}$ defined in (2.3). It follows that a limit cycle is compact and invariant [35, p.106].

2.1.1 Lyapunov Stability of a Periodic Orbit

Lyapunov's results on stability analysis, along with the Barbashin-Krasovsskii-LaSalle invariance principle, provide a powerful framework for analyzing the stability of nonlinear dynamical systems, as well as feedback controllers that guarantee closed-loop system stability [35].

In particular, for systems with an *equilibrium point*, the Lyapunov direct method provides local and global stability conclusions if a continuously differentiable positive-definite function of the nonlinear system states (a Lyapunov function) can be constructed for which its time derivative due to perturbations in a neighbourhood of the system's equilibrium is always negative. The reader is referred to [35] and [43] for overview on elementary results of Lyapunov theory for stability analysis of nonlinear system with an equilibrium point.

Here, we provide an overview of the definition of stability in the sense of Lyapunov, which is specifically applicable for limit cycles. Denote the solution trajectory as:

$$L^+(x_0) = \{x(t, x_0) \mid t \in [0, +\infty)\} \tag{2.4}$$

Denote $B_\delta(x)$ be the open ball with centre x and radius δ.

With this notation, Lyapunov stability is defined as follows: A solution $x(t, x_0)$ to (2.1) system is Lyapunov stable if for each $\epsilon > 0$, there exists $\delta(\epsilon) > 0$ such that for every $y_0 \in B_\delta(x_0)$, the relation:

$$|x(t, x_0) - x(t, y_0)| < \epsilon \qquad \text{holds for all } t \geq 0 \tag{2.5}$$

where $|\cdot|$ is the Euclidean norm. This stability means that if two orbits are near in the beginning, then they remain near together synchronously for all times $t \geq 0$

Similarly, a solution $x(t, x_0)$ to system (2.1) is asymptotically Lyapunov stable if it is Lyapunov stable and there exists $\eta > 0$ such that for every $y_0 \in B_\eta(x_0)$, we yield:

$$||x(t, x_0) - x(t, y_0)|| \to 0 \qquad \text{as } t \to \infty \tag{2.6}$$

2.1.2 Poincaré Return Map and Poincaré stability

Poincaré Theorem [68] is a powerful tool in analysing the stability properties of limit cycles. It provides necessary and sufficient conditions for stability of *periodic orbits* based on the stability properties of a *fixed point* of a discrete-time dynamical system constructed from a Poincaré return map.

For a candidate periodic trajectory, the Poincaré return map is defined by an $(n-1)$-dimensional hyperplane constructed transversal to the periodic orbit. Trajectories starting on the hyperplane close to a point on the periodic orbit will intersect the return map again after a time close to the period of the orbit. This return map essentially traces out the system trajectory from a point on the hyperplane to its next corresponding intersection with the hyperplane. Therefore, the Poincaré return map reduces the stability properties of an n-dimensional dynamical system with periodic solutions to the stability properties of an equilibrium point of an $(n-1)$ discrete-time system.

To verify stability, often a linearization of the return map is computed numerically, and its eigenvalues can be used to verify local orbital stability [54]. However, as we will explore later, it is often impractical to directly apply the Poincaré return map in the analysis of nonlinear system stability because it often cannot be found explicitly, is typically highly nonlinear, multivalued and discontinuous.

Poincaré (or Orbital) stability describes the closeness of two orbits in terms of distance of two sets in the phase space of the system [87]. Define a distance ρ from a point h to the set L as

$$\rho(h, L) = \inf_{y \in L} |h - y| \tag{2.7}$$

where $|\cdot|$ is Euclidean norm in $\mathbb{R}^n$.

Definition 2.3 (Poincaré stability)**.** The system (2.1) is asymptotically stable if for any $\epsilon > 0$, there exists a number $\delta(\epsilon) > 0$ such that for all y_0 satisfying the inequality $|x_0 - y_0| \leq \delta(\epsilon)$, the relation following relation is satisfied:

$$\rho(L^+(x_0), x(t, y_0)) \leq \epsilon, \qquad \forall t \geq 0 \tag{2.8}$$

Definition 2.4 (Asymptotic Poincaré stability)**.** In addition to above, if for some δ_0 and for all y_0 satisfying $|x_0 - y_0| \leq \delta_0$, the following relation holds:

$$\lim_{t \to +\infty} \rho(L^+(x_0), x(t, y_0)) = 0 \tag{2.9}$$

then the trajectory $x(t, x_0)$ is asymptotically Poincaré stable.

2.1.3 Time reparameterization and Zhukovski Stability

A more precise concept of orbital stability is in the sense of Zhukovski [18, 45, 46]. This type of stability is often regarded as Poincaré stability in physical literature since it characterizes also the mutual behaviour of orbits of system (2.1) in phase space [87]. However, while Poincaré stability is a **global** characterization of mutual stability of an orbit, the Zhukovski stability is a **local** characterization of mutual stability of an orbit.

To introduce definition of Zhukovski stability, we need the following set of homeomorphisms (i.e., a continuous map whose inverse exists and is also continuous)

$$Hom = \{\tau(\cdot) \mid \tau : [0, +\infty) \to [0, +\infty), \tau(0) = 0\} \tag{2.10}$$

The functions $\tau(t)$ from the set Hom play the role of the reparameterization of time for the trajectories of the system (2.1).

Definition 2.5 (Zhukovski stability)**.** The trajectory $x(t, x_0)$ of the system (2.1) is Zhukovski stable if for any number $\epsilon > 0$ there exists a number $\delta(\epsilon) > 0$ such that

for any vector y_0 satisfying the inequality $|x_0 - y_0| \leq \delta(\epsilon)$, there exists a function $\tau(\cdot) \in Hom$ such that the following inequality is valid:

$$|x(t, x_0) - x(\tau(t), y_0)| \leq \epsilon \quad \forall t \geq 0 \tag{2.11}$$

Definition 2.6 (Asymptotic Zhukovski stability)**.** If in addition to above, for some number $\delta_0 > 0$ and any y_0 from the ball $\{y \mid \|x_0 - y\| \leq \delta_0\}$ there exists a function $\tau(\cdot) \in Hom$ such that

$$\lim_{t \to +\infty} |x(t, x_0) - x(\tau(t), y_0)| = 0 \tag{2.12}$$

then, the trajectory $x(t, x_0)$ is asymptotically Zhukovski stable.

Proposition 2.1 (Connection between stability in the sense of Lyapunov, Zhukovski and Poincaré)**.** For dynamical system (2.1), Lyapunov stability implies Zhukovski stability and Zhukovski stability implies Poincaré stability.

However, it is important to note that the converse is not true. The three types of stability are equivalent in case of $x(t, x_0)$ being an equilibrium point.

2.1.4 Moving Poincaré Section

Since Zhukovski Stability is the Lyapunov stability of reparameterized trajectories, Zhukovski stability can be explored with methods developed for the study of Lyapunov stability. Based on Zhukovski stability, the *moving Poincaré section*, as introduced in [45], is an extension over the Poincaré return map as described in Section 2.1.2. By introducing not one just one return map but a family of transverse surfaces parameterized by the points on the cyclic trajectories, we essentially "force" the Poincaré section to move along the trajectory $x(t, t_0)$.

The classical Poincaré return map describes the behaviour of trajectories by drawing the intersection points of a trajectory and the hyperplane at discrete moments of time. The reparameterization of time in Zhukovski stability enables the organization of motion along the trajectory such that at a time t, all trajectories cross simultaneously the same moving Poincaré section.

2.1.5 Transverse Linearization and Transverse Lyapunov Theory

In [37, 57, 73], the technique of moving Poincaré section is further extended by taking advantage of the "transversal coordinates" and thereby extending the use of Lyapunov theory for limit cycles.

For a nonlinear system with a stable equilibrium point, the quadratic Lyapunov function derived from its linearization is a valid Lyapunov function for the original nonlinear system [43]. However, [37] shows that this technique cannot be directly applied to exponentially stable limit cycles – even if a periodic orbit is exponentially stable, its linearization will not be exponentially stable. This is because variations tangent to the orbit do not asymptotically converge to zero since they correspond to initial conditions on the orbit. Instead, local stability of an orbit is defined as follows.

Suppose we have dynamical system:

$$\dot{x} = f(x) \tag{2.13}$$

on $\mathbb{R}^n$ and suppose that $\eta \subset \mathbb{R}^n$ is a periodic solution for (2.13) with period T.

Using the distance function:

$$d(x, \eta) := \min_{y \in \eta} \|x - y\| \tag{2.14}$$

An ε-neighbourhood of η can be specified as

$$B_\varepsilon(\eta) := \{x \in \mathbb{R}^n : d(x, \eta) < \varepsilon\} \tag{2.15}$$

The orbit η is stable if trajectories starting near η stay near η. That is, for every $\varepsilon > 0$, there exists $\delta > 0$ such that $x \in B_\delta(\eta) \rightarrow \psi_t^f(x) \in B_\varepsilon(\eta)$ for all $t \geq 0$ (ψ_t^f is the flow of the vector field f). Further, the orbit is exponentially stable (orbitally stable) if it is asymptotically stable and the convergence is exponential. That is, there exists $\delta, M, \lambda > 0$, such that $d(\psi_t^f(x), \eta) \leq d(x, \eta) M e^{-\lambda t}$, for all $x \in B_\delta(\eta)$.

[37] shows that a periodic orbit is exponentially stable if and only if the linearization of the dynamics *transverse* to the orbit are exponentially stable. Based on this principle, [54, 73] proves orbital stability by first constructing a local coordinate system around the orbit which separates tangential and transverse dynamics of the system. Then, an autonomous Lyapunov function is constructed which proves the exponential stability of the periodic orbit.

The method of constructing local coordinates about a periodic orbit is outlined in [37]. These coordinates highlight the tangential and transverse dynamics of the system, with stability determined by analysing the $n-1$ transverse dynamics.

2.2 Stability of Hybrid Systems via Lyapunov-based Theories

Broadly speaking, hybrid systems consist of continuous time and/or discrete time processes interfaced with some logical or decision-making process which may be a function of the state [23]. Examples of hybrid systems include transmission and stepper motors [5, 88], and biologically inspired robot locomotion [57]. This section summarises Lyapunov-based techniques in proving stability of hybrid systems.

The need for separate theories to be developed to analyse the Lyapunov stability of Hybrid system arises from the fact that stability of a hybrid system depends on both the dynamics of the constituent parts, as well as the switching rules. [13] provides ample examples where two globally asymptotically stable systems with a switching scheme that sends all trajectories to infinity. Similarly, an appropriate switching between two unstable system can produce a stable system. Therefore, even if Lyapunov functions exists for each constituent subsystems individually, restrictions need to be imposed on switching to guarantee stability. This section summarises major results in the Lyapunov stability of finite-dimensional hybrid systems.

2.2.1 Multiple Lyapunov Theorem

Introduced in [12] and further reviewed in [13], the multiple Lyapunov theorem imposes restrictions on switching that are sufficient to guarantee stability, enabling the use of multiple Lyapunov functions to prove the overall stability of a hybrid system. Here, we consider systems that switch among vector fields (respectively difference equations) over time or region of state space.

Suppose $S(r), B(r)$ and $\bar{B}(r)$ represent the sphere, ball, and closed ball of Euclidean radius r about the origin in R^n, respectively. Consider the prototypical example for a switched system

$$\dot{x}(t) = f_i(x(t)), \qquad i \in Q = \{1, ...N\} \tag{2.16}$$

Suppose we have a switching sequence, indexed by an initial state:

$$S = x_0; \qquad (i_0, t_0), (i_1, t_1), ..., (i_N, t_N) \tag{2.17}$$

The sequence (2.17), along with (2.16) completely describes the trajectory, according to the rule: (i_k, t_k) means that the system evolves according to $\dot{x}(t) = f_{i_k}(x(t), t)$ for $t_k \leq t < t_{k+1}$. We denote this trajectory by $x_S(\cdot)$.

We can take projections of this sequence onto its first and second coordinates, yielding the sequence of indices:

$$\pi_1(S) = x_0; \qquad i_0, i_1, ..., i_N, ... \tag{2.18}$$

and the sequence of switching times

$$\pi_2(S) = x_0; \qquad t_0, t_1, ..., t_N, ... \tag{2.19}$$

Using switching sequence from (2.17), we define $S|i$ as the endpoints of the times that system i is active in both the continuous- and discrete-time cases.

The interval completion $\mathcal{I}(T)$ of a strictly increasing sequence of times $T = t_0, t_1, ..., t_N, ...$

is the set

$$\mathcal{I}(T) = \bigcup_{j \in \mathbb{Z}_+} [t_{2j}, t_{2j+1}] \tag{2.20}$$

so, $\mathcal{I}(S|i)$ is *the set of times that the ith system is active* (up to a set of measure zero in the continuous-time case). Finally, denote the even sequence of T by $\mathcal{E}(T)$.

We now review the multiple Lyapunov theory.

Definition 2.7 (Lyapunov-like functions)**.** A function V is "Lyapunov-like" function if V is radially unbounded and is a continuous positive definite function (about the origin, 0) with continuous partial derivatives and $V(0) = 0$. Further, the function must satisfy the condition $\dot{V}(x(t)) \leq 0$ for all $t \in \mathcal{I}(t)$. Finally, V must be monotonically non-increasing on $\mathcal{E}(T)$

Theorem 2.1 (Multiple Lyapunov Theory)**.** [12, Theorem 2.3] Suppose we have a candidate Lyapunov functions V_i, for $i = 1, ...N$ for all i, vector fields $\dot{x} = f_i(x)$, with $f_i(0) = 0$. Further, let $\mathcal{S}$ be the set of all switching sequences associated with the system. If for each $S \in \mathcal{S}$, we have that for all i, V_i is Lyapunov-like for f_i and $x_S(\cdot)$ over $S|i$, then the overall system is stable in the sense of Lyapunov.

It is possible to use different conditions on the V_i to ensure stability. An example is given below.

Definition 2.8 (Non-increasing sequence condition)**.** [12, Def 2.6] [88] If there are candidate Lyapunov functions V_i corresponding to f_i for all i, we say they satisfy the sequence non-increasing condition for a trajectory $x(\cdot)$ if

$$V_{i_{j+1}}(x(t_{j+1})) < V_{i_j}(x(t_j)) \tag{2.21}$$

Consider system where the index set is an arbitrary compact set

$$\dot{x} = f(x, \lambda), \qquad x \in K, \qquad \text{compact.} \tag{2.22}$$

Here, $x \in \mathbb{R}^n$, f is globally Lipschitz in x, continuous in λ. Similar to Eq.(2.17), we define switching sequence:

$$S = x_0; \qquad (\lambda_0, t_0), (\lambda_1, t_1), ..., (\lambda_N, t_N) \tag{2.23}$$

Theorem 2.2 (Multiple Lyapunov with Sequence Non-increasing Condition)**.** For a system in (2.22) with $f(0, \lambda) = 0$, for each $\lambda \in K$, suppose we have candidate Lyapunov functions $V_\lambda \equiv V(\cdot, \lambda)$ such that $V : \mathbb{R}^n \times K \to \mathbb{R}_+$ is continuous. Also, define $\mathcal{S}$ be the set of all switching sequences associated with the system.

If, for each $S \in \mathcal{S}$ we have that for all λ, V_λ is Lyapunov-like for f_λ and $x_S(\cdot)$ over $S|\lambda$ and V_λ satisfy the sequence non-increasing condition for $x_S(\cdot)$, then the overall system is stable in the sense of Lyapunov.

2.2.2 Piecewise Quadratic Lyapunov Function (PQLF)

In [41], stability analysis of nonlinear hybrid systems with piecewise affine dynamics was investigated by constructing Lyapunov functions that are piecewise quadratic (PQLF). Importantly, this method relaxes the problem of finding a Lyapunov certificate for hybrid systems to a solution of a convex optimisation problem with a finite-dimensional set of linear matrix inequalities (LMI). The method partitions the state space into a number of closed (possibly unbounded) polyhedral cells with pairwise disjoint interior. This enables the Lyapunov functions to have certain discontinuity, with each Lyapunov function only catering for its respective partition.

However, there are certain drawbacks on the PQLF method. First, PQLF is unable to analyse limit cycles since the method constructs Lyapunov functions directly in the state space. In addition, when partitioning the state space, it is often insufficient to use the natural partition of the system – further refinement of partitions is typically necessary for effective analysis [31]. As the number of dimension increases, the number of partitions required for analysis also increases significantly. Hence, the method does not scale well with the dimension of the system.

2.2.3 Surface Lyapunov Function (SuLF) for Impact Maps

To improve upon the method of PQLF, [30, 31] introduces the notion of Surface Lyapunov functions (SuLF), which infers global properties of Piecewise Linear Systems (PLS) solely by studying their behaviour of switching surface. To facilitate this, the notion of *impact maps* was introduced, which is the mapping between one switching surface to the next switching surface. Then, the method essentially demonstrates overall system stability by proving the impact maps are contracting by constructing surface Lyapunov functions. Compared with PQLF, SuLF enables the analysis of both limit cycles and equilibrium points and is scalable with higher dimensional system. We now present a brief overview of the method.

Suppose we have system $\dot{x} = Ax + B$, part of some larger PLS, defined on some open polytopical set $X \subset \mathbb{R}^n$. Consider the following hyperplanes in the **boundary** of X:

$$S_0 = \{x \in \mathbb{R}^n \ : \ C_0 S x = d_0\} \qquad S_1 = \{x \in \mathbb{R}^n \ : \ C_1 x = d_1\} \tag{2.24}$$

Assume at $t = 0$, x arrives in a subset of S_0 and the PLS switches to the system. The *impact map* is defined as a map from some subset of S_0 to some subset of S_1. Now, suppose S_0^d is some polytopical subset of S_0 where any trajectory starting at S_0^d satisfies $x(t) \in S_1$, for some finite $t \geq 0$. Also, let $S_1^a \subset S_1$ be the set of those points $x_1 = x(t)$.

We are interested in studying the impact map from $x_0 \in S_0^d$ to $x_1 \in S_1^a$. Since both x_0, x_1 belong to switching surfaces, they can be parameterized in their respective hyperplanes. Let $x_0 = x_0^* + \Delta_0$ and $x_1 = x_1^* + \Delta_1$, where $x_0^* \in S_0$, $x_1^* \in S_1$, and Δ_0, Δ_1 are any vectors such that $\Delta_0 \in S_0^d - \{x_0^*\}$ and $\Delta_1 \in S_1^a - \{x_1^*\}$. This reparameterization essentially reduces the map from Δ_0 to Δ_1.

Then, to prove stability of the system, we construct Lyapunov functions V_0 and V_1 on switching surfaces $S_0^d \subset S_0$ and $S_1^a \subset S_1$ respectively such that the following holds.

$$V_1(\Delta_1) < V_0(\Delta_0) \qquad \forall \Delta_0 \in S_0^d - x_0^* \tag{2.25}$$

If V_0 and V_1 exists, then the impact map from S_0^d to S_1^a is a contraction.

2.3 Stability of Hybrid Systems via Contraction Analysis

While the Lyapunov-based theories outlined in the preceding section provide a "certificate" proving existence and stability of limit cycles, these Lyapunov certificates must generally be constructed about a known equilibrium. Therefore, those methods are not applicable when the system dynamics are uncertain, as uncertainty will generally change the location of the limit cycle in state space.

An alternative to Lyapunov-based methods is to search for a *contraction metric*, first developed in [49, 50]. An important advantage of the Contraction Analysis framework over Lyapunov-based methods is that it does not require specific knowledge of the nominal trajectory. Instead, a contraction metric implies the existence of a stable equilibrium indirectly. This section outlines the basics of the Contraction Analysis framework and its application to analysing the stability of limit cycles.

2.3.1 Contraction Analysis for Nonlinear Systems

The Contraction Analysis framework [49, 51] is derived using elementary tools from continuum mechanics and differential geometry. Traditionally, stability is viewed relative to some nominal motion or equilibrium. Contraction Analysis is motivated by the insight that defining stability does not necessarily require prior knowledge of a nominal trajectory - a system is stable if initial conditions or temporary disturbances are somehow "forgotten". That is, if the final behaviour of the system is independent of initial conditions - all trajectories then converge to the nominal motion. Therefore, stability can be analysed differentially by analysing whether nearby trajectories converge to one another.

Consider a system described by a nonlinear deterministic differential equation in the form:

$$\dot{x} = f(x,t) \tag{2.26}$$

where x is the n-dimensional state vector and f is a non-linear vector field. Further, we assume all quantities are real and smooth and any solution $x(x_0,t)$. Under these assumptions, we can obtain the following differential relation from (2.26):

$$\delta\dot{x}(t) = \delta f = \frac{\partial f}{\partial x}(x,t)\delta x \tag{2.27}$$

The $\delta x(t)$ in (2.27) is known as the virtual displacement at a fixed time, and its use is one of the main features of contraction theory. Roughly speaking, virtual displacements of the state x consists of a slight modification of the state to see the change it produces on the velocity vector $\dot{x}$ [42].

Suppose now we define a state dependent local and virtual change of coordinate on (2.27):

$$\delta z = \Theta(x,t)\delta x \tag{2.28}$$

Then, the virtual squared-length in the δz coordinates is:

$$\delta z^T \delta z = \delta x^T M(x,t)\delta x \tag{2.29}$$

where $M(x,t) = \Theta^T\Theta$ is a symmetric, uniformly positive definite and continuously differentiable metric. (Formally, this defines a Riemannian manifold, as per [50]) Further, the generalised virtual dynamics can be expressed in the new δz-coordinate as:

$$\delta\dot{z} = F(x,t)\delta z \tag{2.30}$$

where the generalized Jacobian F is given by:

$$F = \left(\dot{\Theta} + \Theta \frac{\partial f}{\partial x} \right) \Theta^{-1} \tag{2.31}$$

Definition 2.9 (Contraction region)**.** Given system equation (2.26), a region of the state space is called a contraction region with respect to a uniformly positive definite metric $M(x,t)$ in (2.29) if there exists a strictly positive constant β_M such that

$$F = \left(\dot{\Theta} + \Theta \frac{\partial f}{\partial x} \right) \Theta^{-1} \leq -\beta_M I \tag{2.32}$$

or equivalently:

$$\frac{\partial f}{\partial x}^T M(x) + M(x) \frac{\partial f}{\partial x} + \dot{M} \leq -2\beta_M M \tag{2.33}$$

is verified in that region.

Theorem 2.3 (Contraction Theory [51])**.** Given system equation (2.26), any trajectory, which starts in a ball of constant radius with respect to the metric $M(x,t)$ in (2.29) centred at a given trajectory and contained at all times in a contraction region with respect to M_i, remains in the ball and converges exponentially to this trajectory.

The mathematical proof of the above theorem can be found in [51]. Intuitively, the above result means that if the evolution of a virtual displacement tends to zero as time goes to infinity, the whole flow will “shrink" to an equilibrium point - hence the term “contraction”.

2.3.2 Contraction Analysis on Synchronised Oscillators

Contraction theory has also been extended to analyse synchronisation phenomena in distributed networks of nonlinearly coupled oscillators [67, 70, 74, 84]. Generally in these works, a *virtual* axillary system is constructed whose particular solutions include the individual subsystems' states. Proof of synchronization follows from the proof of contracting property with respect to the virtual state variables.

2.3.3 Transverse Contraction for Nonlinear Limit Cycles

In [56], the contraction analysis framework is extended to enable analysis of limit cycles. Solutions starting in a transverse contracting region will converge to a unique limit cycle.

The transverse contraction condition requires the metric to be contracting as per (2.33) whenever the transverse condition $\delta x^T M f = 0$ is satisfied. [56] shows that this condition can be written as a linear matrix inequality. A system (2.26) is transverses contracting if we can search for a symmetric positive-definite matrix function $W(x)$ and a function $\rho(x) \geq 0$ such that:

$$W(x)A(x)^T + A(x)W(x) - \dot{W}(x) + \lambda W(x) - \rho(x)Q(x) \leq 0 \tag{2.34}$$

where $Q(x) = f(x)f(x)^T$. Transverse contraction is a strictly weaker condition than contraction, so every contracting system is also transverse contracting. Therefore, periodic solution to which a transverse contracting system converges may be trivially periodic - i.e., an equilibrium.

2.3.4 Contraction Analysis of Switched or Hybrid Systems

While classical contraction analysis focused on systems with continuously differentiable vector fields, recent extensions for incremental stability of non-differentiable vector fields have been presented in the literature.

[51] discusses the incremental stability of piecewise smooth continuous systems, and of hybrid systems whose switches are fixed in time. The study of such hybrid systems is extended in [26] where dwell-time-based conditions are proposed for exponential convergence of nonlinear nonautonomous resetting systems. In [66], stability of hybrid stochastic systems are discussed using contraction analysis. Note that in these works, hybrid systems whose switches are fixed in time are considered – a simpler case compared to the state-dependent switches considered in this thesis.

In [24, 25, 28], contraction analysis is further applied to the study the incremental stability of different classes of Filippov systems including piecewise smooth systems, piecewise affine systems and relay feedback systems.

2.4 Stability and Robustness Analysis of Walking Robots

The development of legged robots that realise the stability, efficiency and agility of human walking has been the subject of intensive research in recent years (e.g. [21, 33, 85]). Underactuated bipedal "dynamic walkers" can demonstrate amazing feats of efficiency [7], but control design and stability analysis is inherently difficult since their dynamics are highly nonlinear, hybrid (mixing continuous dynamics with discrete impact events), and the target motion is a limit cycle (or more complex trajectory), rather than an equilibrium [33].

The most common approach in studying the stability of periodic bipedal walking motion is via the Poincaré map as discussed in Section 2.1.2 [58] [85]. To measure the robustness of limit cycle walkers, the gait sensitivity norm based on a Poincaré map is used in [39]. In [14], metastability analysis is applied to limit cycle dynamics on the Poincaré map to study robustness to unknown terrain.

However, for models of walking robots, the Poincaré map generally cannot be found explicitly and hence can only be numerically approximated. Further, since the system's evolution is only analysed on a single surface, regions of stability in the full state space are difficult to evaluate. [22] avoids the use of Poincaré map by using the continuous formulation of the hybrid dynamical system to construct a linear robust controller which minimizes the L_2 gain from terrain perturbations. The theoretical contribution of this thesis will enable the study of stability and robustness to parametric uncertainty of nonlinear hybrid limit cycles.

2.5 Semidefinite Optimization for Stability Analysis

Semidefinite programming (SDP) is the optimization of a linear function subject to linear matrix inequality (LMI) constraints. It generalizes several kinds of problems such as linear programming and quadratic programming [10]. SDPs can be solved effectively using interior point methods, which have polynomial worst-case complexity and perform well in practice [86].

A recent important development in SDP is Sum of Squares (SOS) programming [64], which addresses the question of whether there exists a sum of squares decomposition for a given multivariate polynomial. Such a decomposition is a sufficient condition for the polynomial's global nonnegativity.

Testing global nonnegativity of a polynomial function, which is required for applications in Lyapunov theory and contraction theory, is NP-hard. This computational complexity can be avoided by using the sum of squares decomposition as a sufficient condition for global nonnegativity, which can be attained in polynomial time via a SDP.

2.5.1 Sums-of-Squares Programming

As an example on the application of SOS [62], consider the example polynomial from [82]:

$$q(x_1, x_2) := x_1^2 + 2x_1^4 + 2x_1^3 x_2 - x_1^2 x_2^2 + 5x_2^4 \tag{2.35}$$

Equation (2.35) can be represented in *Gram matrix representation* where $p(x) = z^T Q z(x)$ where $z(x)$ is a vector of monomials of degree less than or equal to d, and Q is a symmetric matrix:

$$z(x) := \begin{bmatrix} x_1 \\ x_1^2 \\ x_1 x_2 \\ x_2^2 \end{bmatrix} \tag{2.36}$$

$$Q := \begin{bmatrix} 1 & 0 & 0 & 0 \\ 0 & 2 & 1 & -0.5 \\ 0 & 1 & 0 & 0 \\ 0 & -0.5 & 0 & 5 \end{bmatrix} \tag{2.37}$$

The existence of a symmetric positive semidefinite Q proves the feasibility of a SOS decomposition $p(x)$. Note that the Gram matrix Q is *not unique* due to dependencies among the monomials in z. In this example, $x_1^2x_2^2$ can be expressed as $(x_1x_2)(x_1x_2)$ or $(x_1^2)(x_2^2)$. Therefore, suppose:

$$N := \begin{bmatrix} 0 & 0 & 0 & 0 \\ 0 & 0 & 0 & -0.5 \\ 0 & 0 & 1 & 0 \\ 0 & -0.5 & 0 & 0 \end{bmatrix} \tag{2.38}$$

then $z^T(x)Nz(x) = 0$ for all x, and thus $Q + \lambda N$ also gives a Gram matrix representation of $q, \forall\lambda \in \mathbb{R}$.

We now consider more vigorously the SOS condition and the associated algorithm for decomposition, as introduced in [62].

Definition 2.10 (Sum-of-squares polynomial)**.** A polynomial p of degree $2d$ is an SOS if and only if there exists $Q \succcurlyeq 0$ (positive semidefinite) such that $p(x) = z^T(x)Qz(x), \forall x$, where $z(x)$ is the vector of all monomials of degree up to d.

The above Definition 2.10 follows from the following *equivalent* statements for a polynomial p of degree $2d$ and the vector z of all monomials of degree $\leq d$ as explored in [82]:

1. p is SOS.
2. $\exists$ row vectors $L_1, ..., L_N \in \mathbb{R}^{1\times l_z}$ such that $p(x) = \sum_{i=1}^{N}(L_iz(x))^2, \quad \forall x \in \mathbb{R}^n$
3. There exists a matrix $L \in \mathbb{R}^{N\times l_z}$ such that $p(x) = z^T(x)L^TLz(x), \quad \forall x \in \mathbb{R}^n$

4. There exists a positive-semidefinite matrix Q such that $p(x) = z^T(x)Qz(x)$

Suppose now we parameterize all Gram matrix representations by defining a linear operator $\mathcal{L}$ that maps symmetric matrix Q to the polynomial $z^T(x)Qz(x)$, where $z(x)$ is a vector of monomials of degree up to d. Then, each Gram matrix representation for p is a solution for p is a solution of $\mathcal{L}(Q) = p$. Now, define the matrices $N_1, ..., N_M \in \mathbb{R}^{v \times v}$ where v is the length of $z(x)$, span the null space of $\mathcal{L}$, that is, $\mathcal{L}$ maps each N_i to the zero polynomial and every matrix in the null space of $\mathcal{L}$ is a linear combination of $N_1, ..., N_m$. Then, we get that for every value of $\lambda_i \in \mathbb{R}$, $Q = Q_0 + \sum_{i=1}^{n} \lambda_i N_i$, is a solution to $\mathcal{L}(Q) = p$.

Therefore, p is an SOS iff there exist $\lambda_1, ..., \lambda_m$ such that

$$Q_0 + \sum_{i=1}^{M} \lambda_i N_i \succcurlyeq 0 \tag{2.39}$$

which is a LMI feasibility problem. A matrix representation of $\mathcal{L}$ can be computed since both the domain and range spaces of $\mathcal{L}$ is finite dimensional. Solving $\mathcal{L}(Q) = p$ for a particular solution and $\mathcal{L}(Q) = 0$ for all homogenous solutions, i.e. for $N_1, ..., N_m$, reduces to standard matrix operations.

There exists several software packages for solving SOS programs, including SOSTOOLS [69], YALMIP [47] and Spotless [2]. Both packages are compatible with open-source solver SeDuMi [75] and commercial solver MOSEK.

2.5.2 Generalised S-procedure

In Lyapunov and contraction analyses, we often encounter problems with constraints of the form

$$g_0(x) \geq 0 \tag{2.40}$$

for all x satisfying

$$g_1(x) \geq 0, ..., g_m(x) \geq 0 \tag{2.41}$$

where $g_0, g_1, ..., g_m : \mathbb{R}^n \to \mathbb{R}$. Note that Equations (2.40) and (2.41) can equivalently be written as the set-containment constraint:

$$\{x \in \mathbb{R}^n : \ g_1(x) \geq 0, ..., g_m(x) \geq 0\} \subseteq \{x \in \mathbb{R}^n : g_0(x) \geq 0\} \tag{2.42}$$

The S-procedure is a useful relaxation widely deployed in solving the above problem [82]. We provide an overview here.

Theorem 2.4 (S-procedure)**.** A potentially conservative but useful algebraic sufficient condition for Eqs.(2.40) and (2.41) is the existence of positive-semidefinite functions $s_1, ..., s_m : \mathbb{R}^n \to \mathbb{R}$ such that

$$g_0(x) - \sum_{i=1}^{m} s_i(x) g_i(x) \geq 0 \qquad \forall x \in \mathbb{R}^n \tag{2.43}$$

Proof. Take an arbitrary point x such that $g_1(x) \geq 0, ..., g_m(x) \geq 0$. Then, $g_i(x)s_i(x) \geq 0$ for all $i = 1, ..., m$. Consequently, $g_0(x) \geq 0$ is satisfied due to Eq. (2.43), and the constraints in (2.40) and (2.41) holds. □

For cases in which $g_0, g_1, ..., g_m$ are quadratic functions, the sufficient condition in (2.43) is known as the S-procedure relaxation [11].

2.5.3 Using SOS to search for Lyapunov and Contraction certificates

A combination of SOS techniques, Positivestellensatz and the S-procedure has been applied in finding Lyapunov certificates [81] [82] and contraction metrics [6]. We provide an overview of the method for searching a Lyapunov certificate.

Suppose we have autonomous nonlinear dynamical system:

$$\dot{x}(t) = f\left(x(t)\right) \tag{2.44}$$

where $x(t) \in \mathbb{R}^n$ is the state vector, and the locally Lipschitz function $f : \mathbb{R}^n \to \mathbb{R}^n$ determines the system dynamics. Define $\phi(\xi, t)$ as the solution to (2.44) at time t with the initial condition $\phi(\xi, 0) = \xi$

The region of attraction for the equilibrium $x = 0$ of the system (2.44) is $\{\xi \in \mathbb{R}^n : \lim_{t\to\infty} \phi(\xi, t) = 0\}$. To demonstrate stability, we search for a positive definite Lyapunov function V, such that the following Lemma holds.

Lemma 2.1 (SOS conditions for Lyapunov function)**.** Suppose $\gamma > 0$ and suppose there exists a continuously differentiable function $V : \mathbb{R}^n \to \mathbb{R}$ such that

$$\Omega_{V,\gamma} := \{x \in \mathbb{R}^n : V(x) \leq \gamma\} \quad \text{is bounded} \tag{2.45}$$

$$V(0) = 0, \;\; V(x) \geq 0 \;\; \text{for all nonzero } x \in \mathbb{R}^n \tag{2.46}$$

$$\Omega_{V,\gamma} \backslash \{0\} \subset \{x \in \mathbb{R}^n : \nabla V(x) f(x) < 0\} \tag{2.47}$$

Then, for all $\xi \in \Omega_{V,\gamma}$, the solution $\phi(\xi, \cdot)$ of (2.44) exists on $[0, \infty)$, satisfies $\phi(\xi, \cdot) \in \Omega_{V,\gamma}$ for all $t \geq 0$ and $\lim_{t\to\infty} \phi(\xi, t) = 0$

The S-procedure (as outlined in Section 2.5.2) can be used to verify the above conditions. Using the S-procedure, if $l : \mathbb{R}^n \to \mathbb{R}$ is positive definite and $s : \mathbb{R}^n \to \mathbb{R}$ is positive semidefinite, and

$$-\left[l(x) + \nabla V(x) f(x)\right] + s(x)\left[v(x) - \gamma\right] \geq 0 \qquad \text{for all } x \tag{2.48}$$

then, (2.47) holds.

Proof. Let x be nonzero and satisfy $V(x) \leq \gamma$. Since $s(x) \geq 0$ it follows from (2.48) that $\nabla V(x) f(x) \leq -l(x) < 0$ □

This sufficient condition leads to the following optimisation, which can enlarge the value of γ such that $\Omega_{V,\gamma}$ is an invariant subset of the region of attraction by the choice of positive-semidefinite function s

$$\max_{\gamma,s} \quad \gamma \tag{2.49}$$

subject to

$$s(x) \geq 0 \quad \text{for all } x \tag{2.50}$$

$$-\left[l(x) + \nabla V(x) f(x)\right] + s(x)\left[V(x) - \gamma\right] \geq 0 \quad \text{for all } x \tag{2.51}$$

where V, l are given; the scalar γ and function s are decision variables. [82] provides a worked-example of the above theorems.

2.6 Summary

The control stabilization problem for dynamic walking robots are inherently difficult, due to the nonlinearity, open-loop instability, hybrid (impact) dynamics and limit cycles behaviour which may not be precisely known in advance. This chapter has outlined current stability analysis tools for both hybrid systems and nonlinear limit cycles. These methods require Lyapunov functions to be constructed around a known solution which may not be available in advance for a walking robot.

Recent developments in contraction analysis provide a promising framework for stability analysis for walking robots. Unlike methods based on Lyapunov theory, contraction analysis does not require knowledge of the location of the limit cycle in state space *a priori*. This thesis builds on these results in contraction to develop new stability analysis tools for hybrid nonlinear limit cycles, applicable to the control and stability for walking robots.

Chapter 3

Stability and Robustness of nonlinear hybrid limit cycles via a transverse contraction approach

The results presented in this chapter has been published in the proceedings of IEEE Conference on Decision and Control (2014) entitled "Transverse Contraction for Stability of Nonlinear Hybrid Limit Cycles" ([77]), as well as in a journal article entitled "Transverse Contracting Hybrid Systems and Robust Stability of Dynamic Walking Robots" ([78]) currently under review.

3.1 Introduction

Nonlinear hybrid dynamical systems with periodic solutions are widely found in diverse engineering and scientific fields such as chemistry, electronics and biomechanics, e.g. [16, 27, 72]. These hybrid systems contain continuous-time and discrete, impulsive dynamics which interact with each other. Stability of these dynamical systems is often a fundamental requirement for their practical value in applications.

In this chapter, we address the question: do all solutions of a hybrid nonlinear system

starting in a particular set K converge to a periodic solution, i.e. a unique stable limit cycle?

A major motivation of this work is the study of underactuated bipedal locomotion [21], where even the analysis of stable walking motion on flat ground – i.e. limit cycles in state space – is difficult [85]. This is because the associated dynamics are inherently hybrid due to impacts, and are highly nonlinear [73].

The most well-known stability analysis tool for limit cycles is the Poincaré map [34], which describes the repeated passes of the system through a single transversal hypersurface. However, for nonlinear systems, the Poincaré map generally cannot be found explicitly. Further, since the system's evolution is only analyzed on a single surface, regions of stability in the full state space are difficult to evaluate.

In practice, stability in the full state space is often estimated using cell-to-cell mapping [40], which has been applied to analysis of walking robots [71]. However, computational costs of these methods are exponential in the dimension of the system.

In recent years, convex optimization methods have been widely applied in search for a "stability certificate" based on Lyapunov theory [43]. To characterize regions of stability for limit cycles, [31] and [30] introduced the notion of the Surface Lyapunov function, which verifies stability based on the "impact map" between one switching surfaces to the next switching surface. The method is limited to Piecewise Linear Systems. In [54], nonlinear limit cycle stability analysis was performed by constructing Lyapunov functions in the transverse dynamics.

However, these Lyapunov based methods require knowledge of the exact location of the limit cycle in state space, and hence are not applicable when the system dynamics are uncertain, since uncertainty will generally change the location of the limit cycle.

An alternative approach to Lyapunov methods is to search for a contraction metric [6, 50]. By defining stability incrementally between any two trajectories, contraction analysis answers the question of whether the limiting behaviour of a given dynamical system is independent of its initial conditions.

Contraction theory has been extended to analyse synchronisation phenomena in distributed networks of nonlinearly coupled oscillators in [67, 70, 74, 84]. Generally in these works, a *virtual* axillary system is constructed whose particular solutions include the individual subsystems' states. Proof of synchronization follows from the proof of contracting property with respect to the virtual state variables.

In [24, 25, 28], contraction analysis is further applied to the study the incremental stability of different classes of Filippov systems including piecewise smooth systems, piecewise affine systems and relay feedback systems. For analysis of limit cycles, transverse contraction was first introduced in [56].

In this chapter, we propose a transverse contraction framework for analysis of hybrid limit cycles, building on the work of transversal surface construction in [54], and continuous transverse contraction of [56]. For the purposes of robustness analysis, an important advantage is that Lyapunov functions must be generally constructed around a known equilibrium, whereas a contraction metric derived herein implies existence of a stable equilibrium indirectly. This is vital if the equilibrium may change location depending on unknown dynamics.

This chapter proceeds as follows. Problem formulation and preliminaries are outlined in Section 3.2. In Section 3.3, the transverse contraction conditions guaranteeing stability of a limit cycle in a nonlinear hybrid system is presented. We then formulate convex criteria enforcing these conditions on the nonlinear system in Section 3.4, thereby enabling the search for stability certificates via convex optimisation techniques such as sum-of-squares programming. Using the techniques presented, a framework for robustness analysis for limit cycle is presented in Section 3.5. An illustrative analytical examples on a dynamic walking model is presented in Section 3.6.

3.2 Preliminaries and Problem Formulation

We consider the following class of autonomous hybrid dynamical systems.

$$\dot{x} = f(x) \qquad x \notin S_i^- \tag{3.1}$$

$$x^+ = g(x) \qquad x \in S_i^- \tag{3.2}$$

We define the set K as a non-empty, compact subset of $\mathbb{R}^n$. Further, $x \in K$; f, g are smooth; and $f : K \to \mathbb{R}^n$. We assume x is strictly forward invariant under f, i.e., any solutions of (3.1), (3.2) starting in $x(0) \in K$ is in the interior of K for all $t > 0$.

For simplicity, we assume that the region K is broken into a finite sequence of continuous region in the state space, each denoted K_i for $i = 1, 2, ..., N$; i.e., $K = \bigcup_{i=1}^{N} K_i$. Each K_i is a path-connected region and contains no equilibrium point, i.e., $\forall x \in K_i, f(x) \neq 0$.

We define the switching surface where trajectories 'exits' or 'enters' the i-th section as S_i^- and S_i^+ respectively for $i = 1, 2..., N$. We define each switching surface by $S_i^{\pm} := \{x \mid h_i^{\pm}(x) = 0\}$, each a $(n-1)$-dimensional hypersurface with all $h_i^{\pm}(x)$ smooth. We assume that for $i = 1, ..., (N-1)$, S_i^- maps to S_{i+1}^+; with S_N^- mapping to S_1^+. We assume that S_i^+ does not intersect S_i^- inside K_i, for all i .

Further, assume that $\forall x \in S_i^{\pm}, f(x)^T z_i^{\pm}(x) > 0$ where $z_i^{\pm}(x)$ is the corresponding normal vector of the switching surface $S_i^{\pm}$; i.e., $z_i^{\pm}(x) := \frac{dh_i^{\pm}}{dx}$. Finally, we assume that for all S_i^+, $h_i^+(x) > 0 \; \forall x \in K_i$; while for all S_i^+, $h_i^-(x) < 0 \; \forall x \in K_i$. This means $\forall i$, $z_i^-(x)$ points 'into' K_i for all S_i^-; while $z_i^+(x)$ points 'away' from K_i for all S_i^+.

We denote the solution curve of the system as $\Phi(x_0, t)$, such that $x(t) = \Phi(x_0, t)$ is the solution at time $t > 0$ of the dynamical system with initial state $x(0) = x_0$. If the system exhibits a non-trivial T-periodic orbit, i.e., for a periodic solution x^*, there exists some $T > 0$ such that $x^\star(t) = x^\star(t + T)$ for all t. Such a solution cannot be asymptotically stable, as perturbations in phase are persistent. Instead, *orbital stability* is better posed [36].

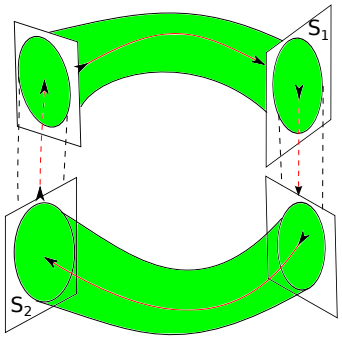

Figure 3.1 – Region of stability around a hybrid limit cycle

The *orbit* of a periodic solution is the set $\mathcal{X}^\star := \{x \in \mathbb{R}^n : \exists t \in [0, T) : x = x^\star(t)\}$. The solution is said to be *orbitally stable* if there exists a $b > 0$ such that for any $x(0)$ satisfying $\text{dist}(x(0), \mathcal{X}^\star) < b$, a unique solution exists and $\text{dist}(\Phi(x_0, t), \mathcal{X}^\star) \to 0$ as $t \to \infty$.

Our goal is to verify that, in our hybrid system (3.1), (3.2), all solutions starting in the particular region K are orbitally stable and converge to a unique limit cycle. This is illustrated in Fig 3.1 for a system with two continuous phases and two switching surfaces. The verified region is shaded green, and the stable limit cycle in red. Continuous dynamics are shown in solid line with discrete impulse between switching surfaces shown in dotted line.

To achieve our goal, we will present extensions of contraction analysis [50] specifically for hybrid limit cycles.

We will hereafter refer to the Jacobian of f as $A(x) := \frac{\partial f}{\partial x}$.

For completeness, we now restate the transverse contraction condition for continuous systems derived in [56]. It was shown in [56] that if a system is transverse contracting, then all solutions starting with $x(0) \in K$ are stable under time reparameterization, or "Zhukovski stable" [45], and hence converge to a unique limit cycle. We assume a Riemannian distance metric $M(x)$ which is symmetric positive-definite for all x.

Condition 3.1 (Transverse Contraction)**.** A continuous system $\dot{x} = f(x)$ is transverse

contracting with rate λ if there exists a Riemannian metric $M(x)$ satisfying

$$\dot{M}(x) + \frac{\partial f}{\partial x}^T M(x) + M(x)\frac{\partial f}{\partial x} + 2\lambda M(x) \leq 0 \tag{3.3}$$

for all $\delta_x \neq 0$ such that $\delta_x^T M(x) f = 0$.

The latter condition requires δ_x to be transverse to the flow of the system, i.e., δ_x and $f(x)$ are *orthogonal* with respect to the metric $M(x)$. We hereafter refer this as the *orthogonality condition.*

We will derive two methods of enforcing this *orthogonality condition* for hybrid limit cycles in this thesis. First, in section 3.3 and 3.4 we explore embedding the condition directly into the search for the metric M itself. Second, in Chapter 4, we explore defining orthorgonality through the construction of a new coordinate system around a known trajectory. The former results in a n-dimensional metric, M, while the latter results in a $(n-1)$-dimensional metric, $M_\perp$.

3.3 Contraction Conditions for Limit Cycles in Hybrid Systems

In this section, we derive the transverse contraction conditions for hybrid nonlinear limit cycles with a n-dimensional metric, M, and show that these conditions guarantee the stability of a unique limit cycle within a particular set K.

We first present the conditions on the discrete part of the systems which enables proof of a unique stable limit cycle for the hybrid system.

Condition 3.2 (Condition on M on switching surface)**.** Given switching surface $S_i := \{x | h_i(x) = 0\}$, $\forall x \in S_i^-$,

$$\delta_x^T z_i(x) = 0 \Longrightarrow \delta_x^T M(x) f(x) = 0 \tag{3.4}$$

where $z_i(x) := \frac{dh_i}{dx}$ is the normal vector for S^-.

Note that if Condition 3.2 is satisfied, according to the Riemannian metric $M(x)$, all trajectories approach the switching surface orthogonally. This is true since the direction vector of any trajectory on the switching surface $x \in S_i^-$ is given by $f(x)$.

Condition 3.3 (Metric condition on discrete dynamics)**.** The discrete part of the system in Eq. (3.2) satisfies

$$\delta_x^T \left(\frac{\partial g}{\partial x}^T M(g(x)) \frac{\partial g}{\partial x} - M(x) \right) \delta_x \leq 0 \tag{3.5}$$

for all $\delta_x^T M(x) f(x) = 0$ and $x \in S_i^-$.

Theorem 3.1 (Orbital Stability for Hybrid Limit Cycles)**.** Consider the system (3.1),(3.2) which are in a strictly forward invariant set K. If, there exists a metric $M(x)$ which satisfies the following three criteria:

i) the continuous part(s) of the system in Eq. (3.1) are all transverse contracting according to Definition 3.1 w.r.t. $M(x)$;

ii) $M(x)$ satisfies Condition 3.2 on all switching surface(s); and

iii) the discrete part(s) of the system $g(x)$ satisfies Condition 3.3 w.r.t. $M(x)$;

then, all solutions starting in any particular K_i converge to a unique limit cycle that is orbitally stable.

Proof. The proof will be presented in 2 steps.

1. The conditions stipulate all trajectories in any particular K_i are stable under some time-reparameterization, i.e., all trajectories are stable in the sense of Zhukovski;

2. Therefore, there exists a unique limit cycle that is orbitally stable.

These two steps will now be respectively presented in Lemma 3.1 and 3.2. □

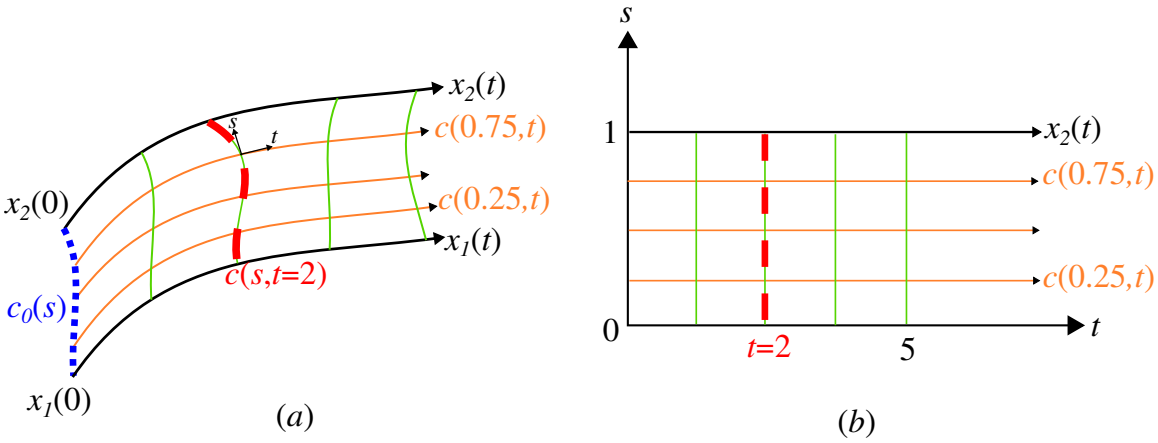

Figure 3.2 – Illustration of the parameterization of a path, $c(s,t)$, between $x_1(t)$, $x_2(t)$. In (a) $x_1(t), x_2(t)$ is shown under the system vector field. $c(s,t)$ is a path connecting the two trajectories. In (b) under the s,t parameterization, the evolution of the path under system dynamics can be represented as a 2-dimensional surface $\mathbf{Q}$. A line of constant t is highlighted in red on the left on the system vector field and on the right for the 2-dimensional surface parameterized by s,t.

Lemma 3.1 (Zhukovski Stability)**.** If the conditions of Theorem 3.1 are satisfied, for every pair of solutions $x_1(t)$ and $x_2(t)$ starting in any K_i, there exists time reparameterization $\tau(t)$ such that $x_1(t) \to x_2(\tau(t))$ as $t \to \infty$. That is, all solutions are stable in the sense of Zhukovski.

Proof. Suppose there are two initial conditions $x_1(0), x_2(0) \in K_i$ for a particular i. We pick any arbitrary smooth path $c_0(s)$, where $c_0(s) : [0,1] \to K_i$ connecting these two initial conditions, such that $c_0(0) = x_1(0)$ and $c_0(1) = x_2(0)$.

We now define $c(s,t) : [0,1] \times \mathbb{R}_+ \to K$ with initial condition $c(s,0) = c_0(s)$ and boundary conditions $c(0,t) = x_1(t)$ and $c(1,t) = x_2(t)$. The path evolves in time with system dynamics for each $s \in [0,1]$ s.t. $\frac{d}{dt}(c(s,t)) = f(c(s,t))$. By smoothness of f and c_0, we have $\frac{\partial c}{\partial s} \neq 0$, $\forall s,t$. Therefore, the evolution of this path under system dynamics can be represented by a 2-dimensional surface parameterized by s and t as shown in Fig 3.2. We denote this 2-dimensional surface as a sub-manifold $\mathbf{Q}$ of K_i.

We now demonstrate for $s \in (0,1]$, we can construct a new curve $\bar{c}(s,t)) : [0,1] \times \mathbb{R}_+ \to K$ which always locally satisfies the orthogonality condition, i.e. $\frac{d\bar{c}(s,t)}{ds}^T M(\bar{c}(s,t)) f(\bar{c}(s,t)) = 0, \forall s,t$. We will further demonstrate the *existence* and *uniqueness* of such path $\bar{c}(s,t)$

in $\mathbf{Q}$. This will be achieved in the following 2 steps:

1. We construct tangent vector field $\delta_\perp(x)$, which is *unique* for each $x = c(s,t) \in \mathbf{Q}$.

2. We construct the path $\bar{c}(s,t)$ by integrating along the tangent vector $\delta_\perp$ we had constructed. We demonstrate that such path $\bar{c}(s,t)$ exists and a unique path passes through each $x = c(s,t) \in \mathbf{Q}$.

First, we construct a tangent vector field, $\delta_\perp(x)$ at each $x = c(s,t) \in \mathbf{Q}$. Consider the tangent plane of $\mathbf{Q}$ evaluated at x, $\mathbf{T}_x\mathbf{Q}$, which is spanned by basis vectors in the direction of $\frac{dc(x)}{ds}$ and $f(x)$. Hence, in general a tangent vector $\delta_\perp(x)$ takes the form:

$$\delta_\perp(x) = \delta_\perp(c(s,t)) = \frac{dc}{ds}\delta_s + f(x)\delta_t. \tag{3.6}$$

We fix $\delta_s = 1$, i.e., the s component of $\delta(x)$ is equal to that of $c(x)$; whereas the t component of $\delta(x)$ advances in the direction of $f(x)$ scaled by δ_t to be derived below. We additionally impose the orthogonality condition on $\delta_\perp(x)$:

$$\delta_\perp(x)^T M(x) f(x) = 0 \tag{3.7}$$

Hence, substituting (3.6) to (3.7), we yield the definition of δ_t:

$$\left[\frac{dc}{ds} + f(x)\delta_t\right]^T M(x) f(x) = 0 \tag{3.8}$$

$$\delta_t = \frac{-\frac{dc}{ds} M(x) f(x)}{f(x)^T M(x) f(x)}. \tag{3.9}$$

Since $f(x) \neq 0$ and $M > 0$, (3.9) and (3.6) uniquely defines $\delta_\perp(x)$, for all $x \in \mathbf{Q}$.

Second, using the vector field defined by $\delta_\perp(x), \forall x = c(s,t) \in \mathbf{Q}$, we can define the path $\bar{c}(s,t)$ by integrating along $\delta_\perp(c(s,t))$ over s:

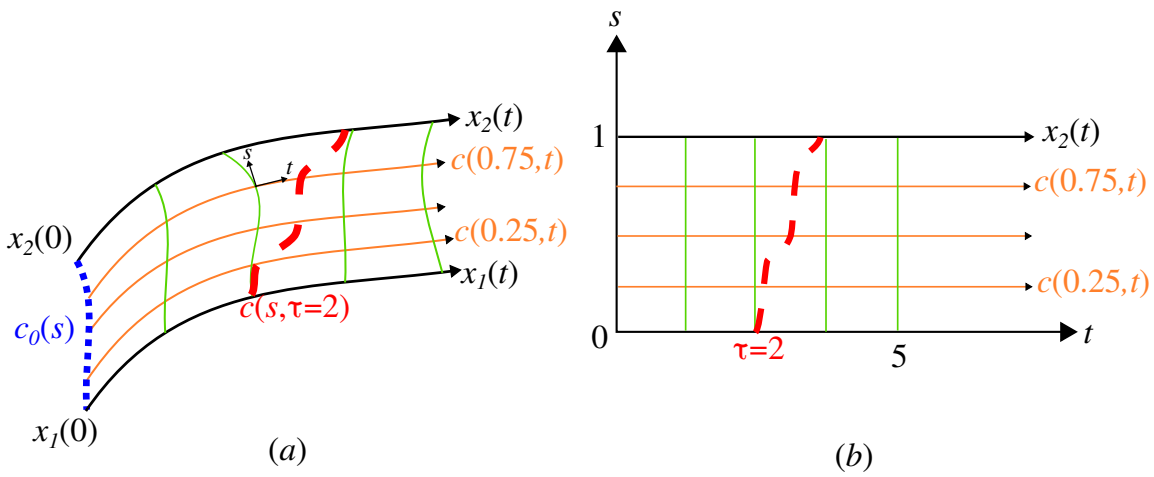

Figure 3.3 – The line $\bar{c}(s,2)$ is highlighted in red on the left on the system vector field and on the right for the 2-dimensional surface parameterized by s,t.

$$\bar{c}(s,t) = \int_0^s \delta_\perp(c(\sigma,t))d\sigma. \tag{3.10}$$

with initial condition for $s = 0$ defined as:

$$\bar{c}(0,t) = x_1(t). \tag{3.11}$$

Due to uniqueness of solution for planar differential equations which are smooth and Lipschitz, there exists a unique path $\bar{c}(s,t)$ with tangent vector $\delta_\perp(x)$ passing through each point $x = c(s,t)$.

Note that by the construction of $\delta_\perp(x)$, the s component of $\bar{c}(s,t)$ remains unchanged from $x = c(s,t)$, while the t component is *reparameterised* to satisfy the orthogonality condition. We define such time reparameterization $\tau(s,t)$, where for $s = 0$, $\tau(0,t) = t$. For $s \in (0,1]$, $\bar{c}(s,t) = c(s,\tau(s,t))$. Hence, we have constructed a unique time reparameterization $\tau(s,t)$ which forms the path $c(s,\tau(s,t))$ satisfying the orthogonality condition $\frac{dc(s,\tau(s,t)}{ds} M(s,\tau(s,t))f(s,\tau(s,t)) = 0$, $\forall s,t$. An example curve of $\bar{c}(s,2)$ is shown in Fig 3.3.

Another result of the uniqueness of such time reparameterised curve is that the mapping $t \mapsto \tau(s,t)$ is homomorphic $\forall s$. Hence, for any given s, we yield that $\tau(s,t)$ is

monotonically increasing w.r.t. t, that is,

$$\dot{\tau}(s,t) > 0, \qquad \forall s,t. \tag{3.12}$$

We now consider the switching surface. Since this path $c(s,\tau(s,t))$ is unique for each $x \in \mathbf{Q}$, and on each switching surface the same orthogonality condition is satisfied by the criterion *(ii)* in Theorem 3.1, we can hence deduce that each switching surface coincide with the curve $c(s,\tau(s,t))$ at a given fixed τ. This result also ensures that no impact occurs between $c_0(s)$ and $\bar{c}(s,0)$. Therefore, combining the continuous phase and discrete phase, the path $c(s,\tau(s,t))$ under τ-parameterization is smooth and remain connected across the switching surface.

We now show that such time-reparameterized path is always shrinking when the conditions of Theorem 3.1 are satisfied. Consider $c(s,\tau)$ and its length, l, under the Riemannian metric $M(x)$ and associated distance function metric $V(x,\delta_x) = \delta_x^T M(x)\delta_x$. During continuous time dynamics, the time derivative of length l is given by:

$$\frac{d}{dt}l(c(s,\tau)) = \int_0^1 \frac{d}{dt}\left[V\left(c(s,\tau), \frac{\partial}{\partial s}c(s,\tau)\right)\right] ds. \tag{3.13}$$

During the discrete switching events, the length is guaranteed to be non-increasing if:

$$\begin{gathered} l^+(c(s,\tau^+)) \leq l^-(c(s,\tau^-)) \\ \int_0^1 V\left(c(s,\tau^+), \frac{\partial}{\partial s}c(s,\tau^+)\right) ds \leq \int_0^1 V\left(c(s,\tau^-), \frac{\partial}{\partial s}c(s,\tau^-)\right) ds. \end{gathered} \tag{3.14}$$

We first study $l(s,\tau)$ under continuous dynamics. Consider, pointwise, the integrand of the right hand side of Equation (3.13):

$$\frac{d}{dt}(\delta_x^T M \delta_x) = \delta_x^T \dot{M} \delta_x + 2\delta_x^T M \dot{\delta}_x \tag{3.15}$$

evaluated at $x = c(s,t)$ and $\delta_x = \frac{\partial c(s,t)}{\partial s}$, i.e.

$$\dot{x} = f(c(s,t))\dot{\tau}(s,t) \tag{3.16}$$

$$\dot{\delta}_x = \frac{\partial f(c(s,t)))}{\partial x}\delta_x\dot{\tau} + f(c(s,t))\frac{\partial \dot{\tau}}{\partial s}. \tag{3.17}$$

Substituting (3.16), (3.17) to (3.15), we yield

$$\frac{d}{dt}(\delta_x^T M \delta_x) = \\ \delta_x^T \dot{M}\delta_x + 2\delta_x^T M \left[\frac{\partial f(c(s,t)))}{\partial x}\delta_x\dot{\tau} + f(c(s,t))\frac{\partial \dot{\tau}}{\partial s}\right].$$

Note that due to the orthogonality condition $\delta_x^T M f = 0$, the last term of the above equation goes to zero, hence:

$$\frac{d}{dt}(\delta_x^T M \delta_x) = \delta_x^T \dot{M}\delta_x + 2\delta_x^T M \left[\frac{\partial f(c(s,t)))}{\partial x}\delta_x\dot{\tau}\right] \tag{3.18}$$

$$= \delta_x^T \left(\frac{\partial M}{\partial x} f\dot{\tau} + 2M\left[\frac{\partial f(c(s,t)))}{\partial x}\dot{\tau}\right]\right)\delta_x. \tag{3.19}$$

Knowing that $\dot{\tau} > 0$ from (3.12), we can factoring out $\dot{\tau}$ and (3.19) is guaranteed to be uniformly negative in the continuous phase of the system by condition (i) of Theorem 3.1.

We now study $l(s,\tau)$ under discrete switching dynamics. Consider, pointwise, the integrands on both sides of (3.14), as shown below:

$$\delta_x^+ M \delta_x^+ < \delta_x^- M \delta_x^- \tag{3.20}$$

$$\delta_x^{-T}\left(\frac{\partial g}{\partial x}^T M \frac{\partial g}{\partial x} - M\right)\delta_x^- \leq 0. \tag{3.21}$$

By condition (iii) of Theorem 3.1, (3.21) is guaranteed to be satisfied and therefore

$l(s,\tau)$ is guaranteed to be non-increasing over the discrete part(s) of the system.

Therefore, $l(s,\tau) \to 0$ as $t \to \infty$. Hence, $x_1(t) \to x_2(\tau(t))$ as $t \to \infty$.

□

Lemma 3.2 (Orbital Stability)**.** If all conditions of Theorem 3.1 are satisfied, there exists a unique limit cycle that is orbitally stable.

Proof. Since K is strictly forward invariant and compact, it follows that the omega-limit set, $\Omega(x)$, exists and is a compact subset of K. Further, an implication of Lemma 3.1 is that all points in K have the same ω-limit set, which we denote $\Omega(K)$.

Pick a point $x^\star$ in $\Omega(K)$, by strict forward invariance, this is an interior point of K. We know that $f(x^\star) \neq 0$, otherwise the results of [50] prove convergence to an equilibrium (see Section 2.3.1). Construct a hyperplane orthogonal to $f(x^\star)$, which we denote by H. We prove convergence to a limit cycle by constructing a Poincaré map on H.

Since $f(\cdot)$ is smooth, for x in some neighbourhood B of $x^\star$ we have that $f(x)^T f(x) > 0$, so in $B_H := B \cap H$ solution curves are transversal to H and pass through it in the same direction as at $x^\star$.

Since $x^\star$ is in the ω-limit set for all points in K, and B_H is transversal, the evolution of the system from any point $x(t) \in B_H$ eventually passes through B_H again. That is, $x(t+s) \in B_H$ where $s > 0$ depends on x. This evolution can be represented by a Poincaré map $T : B_H \to B_H$.

Take the distance between two points $d(x_1, x_2)$ in B_H to be the Riemannian metric distance from Lemma 3.1. By Lemma 3.1, we have that $d(T(x_1), T(x_2)) < d(x_1, x_2)$. Hence, T is a contractive map from B_H unto itself. By the Banach fixed point theorem it has a unique stable fixed point, which is its only limit point so must be $x^\star$. By standard results on Poincaré maps this implies that $x^\star$ is a point on a limit cycle, to which all solutions converge, by Lemma 3.1. □

3.4 Convex Criteria for Limit Cycle Stability in Hybrid Systems

In this section, we give convex conditions for transverse contraction of hybrid systems via a n-dimensional metric, M, enabling the search for the metric via sum-of-squares programming for systems with polynomial dynamics.

For the continuous phase, we first state a convex condition that is necessary and sufficient for transverse contraction derived in [56] for smooth continuous systems.

Definition 3.1 (Convex Criterion for Transverse Contraction)**.** A system $\dot{x} = f(x)$ is transverse contracting with rate λ and a metric $V(x, \delta_x) = \delta_x^T M(x)\delta_x$ if and only if there exists a function $W(x) := M(x)^{-1}$ and $\rho(x) \geq 0$ such that

$$W(x)A(x)^T + A(x)W(x) - \dot{W}(x) + 2\lambda W(x) - \rho(x)Q(x) \leq 0 \tag{3.22}$$

where $Q(x) := f(x)f(x)^T$.

We now derive stability conditions for the switching phase of the hybrid system which are convex.

Theorem 3.2 (Metric Condition linear in W)**.** Suppose the normal vector of the switching surface is $z(x)$. If the Riemannian metric M and the continuous dynamics f satisfies

$$\alpha(x)f(x) - W(x)z(x) = \beta(x)c(x) \tag{3.23}$$

for some scalar function $\alpha(x) > 0$ and some vector function $\beta(x)$; then Condition 3.2 is satisfied and all trajectories approach the switching surface orthogonally.

Proof. For the orthogonality condition of (3.4) in Condition 3.2 to hold, we require $f^T M(x)\delta_x = 0$ to hold for all $z(x)^T\delta_x = 0$. This is equivalent to requiring for some scalar $\alpha(x) > 0$, the following holds

$$z(x)^T = \alpha(x)f(x)^T M(x) \tag{3.24}$$

for all $x \in S$. Reformulating this in terms of $W := M^{-1}$ we yield the requirement

$$\alpha(x)f(x) = W(x)z(x) \tag{3.25}$$

for all $c(x) = 0$. Using the S-procedure formulation [62], we yield the equivalent equality constraint with multiplier $\beta(x)$:

$$\alpha(x)f(x) - W(x)z(x) = \beta(x)c(x) \tag{3.26}$$

which is the required condition for all x. □

Theorem 3.3 (Convex Conditions for Limit Cycle Stability in Hybrid Nonlinear Systems)**.** Suppose, firstly, there exists a Riemannian metric $M(x)$ for nonlinear system (3.1) and (3.2) which satisfies Condition 3.2; secondly, the continuous dynamics of the system satisfies (3.22) in Definition 3.1; and thirdly, the discrete switching dynamics $g(x)$ of the system satisfies the following LMI

$$\begin{bmatrix} W(x) + \zeta(x)Q(x) & W(x)\frac{\partial g}{\partial x}^T \\ \frac{\partial g}{\partial x}W(x) & W(x) \end{bmatrix} \geq 0. \tag{3.27}$$

For some $\zeta(x) \geq 0$, then the overall hybrid system is contracting with respect to metric M.

Proof. We prove contraction by showing the convex conditions satisfies all requirements stipulated in Theorem 3.1. First, by Condition 3.2, the requirements of Condition 3.2 are satisifed.

We require the following condition to be satisfied in Condition 3.3:

$$\delta_x^T \left(\frac{\partial g}{\partial x}^T M \frac{\partial g}{\partial x} - M \right) \delta_x \leq 0 \tag{3.28}$$

for all $\delta_x^T M f = 0$ and $x \in S_i^-$.

Reformulating in terms of the gradient of the metric, i.e. $\eta := M(x)\delta_x$ such that $\delta_x = M^{-1}\eta := W\eta$, we yield the equivalent condition:

$$\eta^T \left(W \frac{\partial g}{\partial x}^T W^{-1} \frac{\partial g}{\partial x} W - W \right) \eta \leq 0. \tag{3.29}$$

The transversality condition $\delta_x^T M f = 0$ becomes $\eta^T f(x) = 0$. Now, define matrix function $Q(x) := f(x)f(x)^T$ which is rank-one and positive-semidefinite. Hence the sets $\{\eta : \eta^T f(x) = 0\}$, $\{\eta : \eta^T Q \eta = 0\}$ and $\{\eta : \eta^T Q(x) \eta \leq 0\}$ are equivalent.

Using this reformulation, the transverse contraction of the discrete switching can be proved by the existence of $W(x)$ such that:

$$\eta^T Q(x)\eta \leq 0 \Rightarrow$$
$$\eta^T \left(W \frac{\partial g}{\partial x}^T W^{-1} \frac{\partial g}{\partial x} W - W \right) \eta \leq 0. \tag{3.30}$$

By the S-procedure, (3.30) is only true if and only if there exists $\zeta(x) \geq 0$ such that

$$\eta^T \left(W + \zeta(x) Q(x) - W \frac{\partial g}{\partial x}^T W^{-1} \frac{\partial g}{\partial x} W \right) \eta \geq 0. \tag{3.31}$$

Using the Schur Complement, (3.31) is true if and only if (3.27) holds. Hence, all conditions of Theorem 3.1 are satisfied which completes the proof. □

Note that these conditions are all linear in the unknown functions $W(x), \alpha(x), \beta(x), \rho(x)$, and $\zeta(x)$, i.e., it consists of a linear matrix inequality at each point x. For polynomial systems, these conditions can be verified efficiently using sum-of-squares (SOS) programming and Positivstellensatz arguments [76].

3.5 Robust Stability analysis for Hybrid Limit Cycles

The contraction framework is especially suitable for uncertain systems where the limit cycle location changes with parametric uncertainty. This is because the framework eliminates the need for linearization or the need to know the exact location of the limit cycle, which often changes with uncertainty.

Consider the hybrid system with parametric uncertainty.

$$\dot{x} = f_\delta(x, \delta) = f_0(x) + \delta f_1(x) \qquad x \notin S_i^- \tag{3.32}$$

$$x^+ = g_\delta(x, \delta) = g_0(x) + \delta g_1(x) \qquad x \in S_i^- \tag{3.33}$$

where δ is some parametric uncertainty.

Robustness to parametric uncertainty can be ascertained by verifying the contraction conditions are satisfied for any given range δ. There is an obvious trade-off between the volume of the stability region and the magnitude of the uncertainty – maximising the stability region volume necessarily decreases the allowable uncertainty magnitude and vice versa. The set of optimal values for these two variables form a *Pareto frontier* as illustrated in Fig 3.4.

There are two options in optimising for a useful uncertainty:

1. Fix a desired stability region and maximise the allowable uncertainty magnitude within the said region; or
2. Fix a particular desired uncertainty magnitude and maximise the volume of the stability region which allows for said uncertainty.

Some combination of the two options can also be used. We now illustrate how these two options can be implemented numerically.

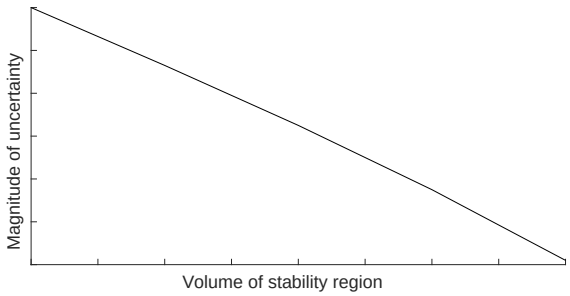

Figure 3.4 – Typical trade-off between stability region volume and the magnitude of allowable uncertainty, which forms a Pareto frontier for the set of optimal values. The plot shows allowable magnitude of uncertainty in the hip viscous friction for varying regions of guaranteed stability of a compass gait biped. This example will be discussed in detail in Section 4.6.

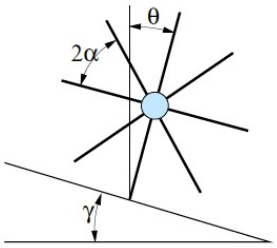

Figure 3.5 – The rimless wheel model

The first option can be implemented by using the same contraction metric for the nominal undisturbed system, then maximise (or minimise) the allowable error which maintains contraction. That is, find the largest (or smallest) δ which satisfies the contraction condition with dynamics from (3.32), (3.33).

The second option can be implemented by searching for a new metric which maximises the uncertainty intervals on the error. This can be achieved using the S-procedure with Lagrange multipliers. Implementation of these methods are further discussed in Section 4.5.

3.6 Application Example

The rimless wheel is a simple planar model of dynamic walking, exhibiting hybrid (switching) behaviour. It consists of a central mass, of mass g, with equally spaced spikes, of length l extending radially outwards. The system rolls down an incline of pitch γ, as shown in Fig. 3.5.

At any given moment, the rimless wheel rotates about the stance foot without slipping, behaving like an inverted pendulum. When the next foot contacts the ground, it is assumed that an elastic collision occurs such that the old stance foot lifts off and the system now rotates about the new stance foot.

The Rimless Wheel state space $x = [\theta, \dot{\theta}]^T$ can be represented with the following

hybrid system dynamics:

$$\frac{d}{dt}\begin{bmatrix}\theta\\ \dot{\theta}\end{bmatrix} = f(\theta,\dot{\theta}) = \begin{bmatrix}\dot{\theta}\\ \frac{g}{l}\sin\theta\end{bmatrix} \qquad \text{for } \theta-\gamma-\alpha \neq 0 \tag{3.34}$$

$$\begin{bmatrix}\theta^+\\ \dot{\theta}^+\end{bmatrix} = g(\dot{\theta}^-) = \begin{bmatrix}\gamma-\alpha\\ \cos(2\alpha)\dot{\theta}^-\end{bmatrix} \qquad \text{for } \theta-\gamma-\alpha = 0. \tag{3.35}$$

On a sufficiently inclined slope, the system has a stable limit cycle, for which the energy lost in collision is perfectly compensated by the change in potential energy. The system has been studied extensively and its basin of attraction has ben computed exactly. [20]

Figure 3.6 shows the phase portrait of the rimless wheel, with blue arrows indicating the direction of the continuous dynamics. The dotted line on the right of the graph indicates the collision surface that maps to the left edge of the graph (or vice-versa, depending on the direction of dynamics). The grey and red lines represent the homoclinic orbits of the system and the stable limit cycle respectively. Using the method outlined in Section 3.4 and convex conditions in Theorem 3.3, we formulate SOS and Positivestellansatz conditions which verifies transverse contraction for the hybrid system in a region defined by the switching surfaces and a Bézier polynomial $b(x)$.

Let $H = A(x)W(x)+W(x)A(x)^T-\dot{W}(x)+2\lambda W(x)$. We approximate the continuous dynamics $f(x)$ with a third order taylor series expansion.

The conditions verified are given below.

$$\begin{aligned} W(x) - (f(x)^T f(x)-\epsilon)L_1(x)& \\ -(\theta-(\gamma-\alpha))L_2(x)& \\ -((\alpha+\gamma)-\theta)L_3(x)& \\ -(\dot{\theta}-b(x))L_4(x) \in SoS& \end{aligned} \tag{3.36}$$

$$\alpha f(x) - W(x)\nabla c = \beta(x)c(x) \tag{3.37}$$

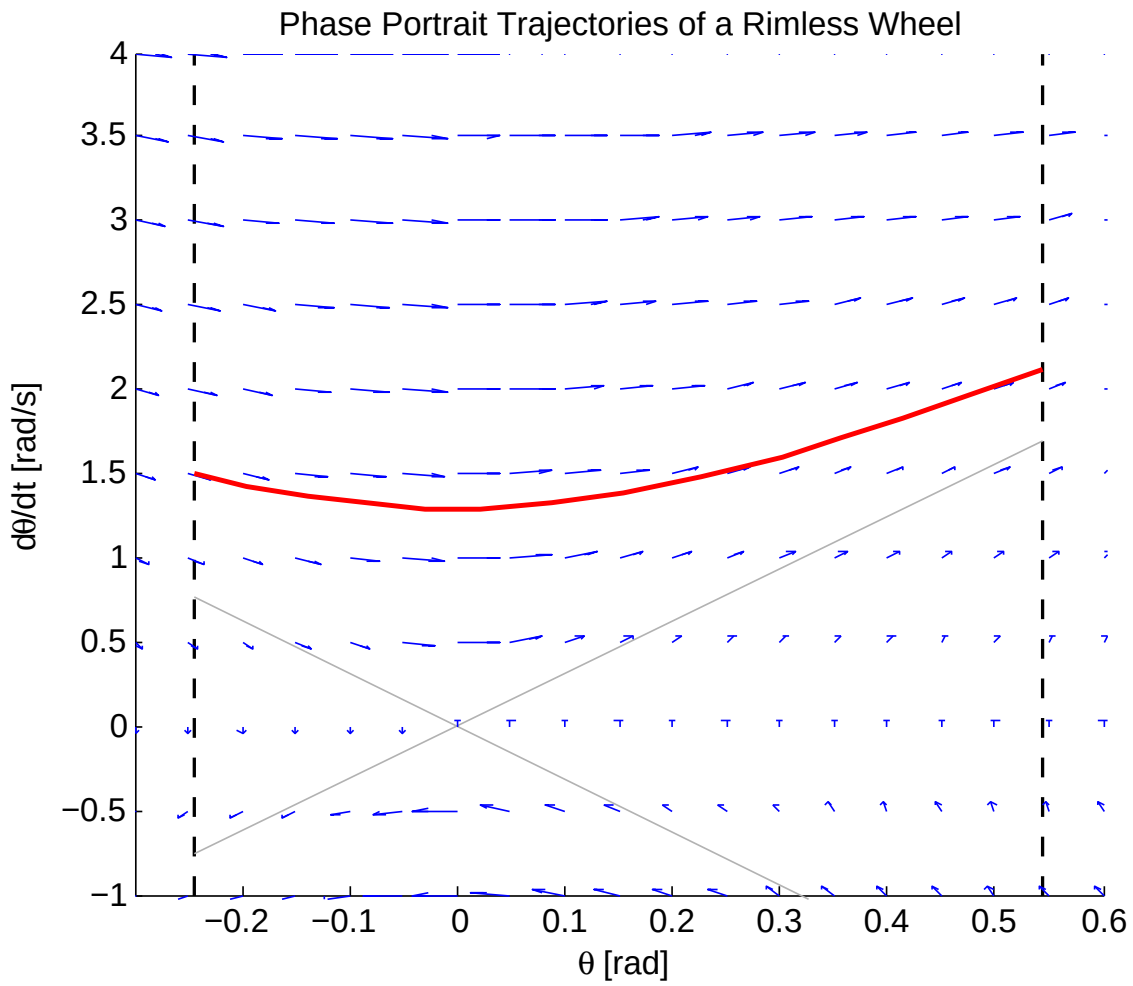

Figure 3.6 – Phase diagram of the rimless wheel model

$$\begin{aligned} &-H - \rho(x)f(x)f(x)^T \\ &-(f(x)^T f(x) - \epsilon)L_5(x) \\ &-(\theta - (\gamma - \alpha))L_6(x) \\ &-((\alpha + \gamma) - \theta)L_7(x) \\ &-(\dot{\theta} - b(x))L_8(x) \in SoS \end{aligned} \tag{3.38}$$

$$\begin{bmatrix} W(x) + \zeta(x)Q(x) & W(x)\frac{\partial g}{\partial x}^T \\ \frac{\partial g}{\partial x}W(x) & W(x) \end{bmatrix} \in SoS \tag{3.39}$$

$$L_1, L_2, L_3, L_4, L_5, L_6, L_7, L_8, \beta(x) \in SoS \tag{3.40}$$

$$\alpha(x), \rho(x), \zeta(x) \in SoS \tag{3.41}$$

(3.36) verifies the positive-definiteness of W within the defined region; (3.37) verifies Condition 3.2; (3.38) and (3.39) verifies the conditions of Theorem 3.3; and, finally, (3.40) and (3.41) verifies positive semi-definiteness of the Lagrange multipliers and scalar functions.

The above conditions were formulated in YALMIP [47, 48] and solved by commercial SDP solver MOSEK v.8.0. The code has been made available online [3]. We found that these conditions could be verfified with $W(x)$ and $\beta(x)$ a matrix of degree-four polynomials, and $L_i(x), \alpha(x), \zeta(x), \rho(x)$ degree-two. Figure 3.7 shows verified regions of stability coloured in green.

3.7 Conclusion

We have derived differential conditions guaranteeing the orbital stability of nonlinear hybrid limit cycles. These conditions are presented as pointwise linear matrix inequalities, enabling an efficient search for a stability certificate.

The main advantages of this approach over traditional Lyapunov-based methods are

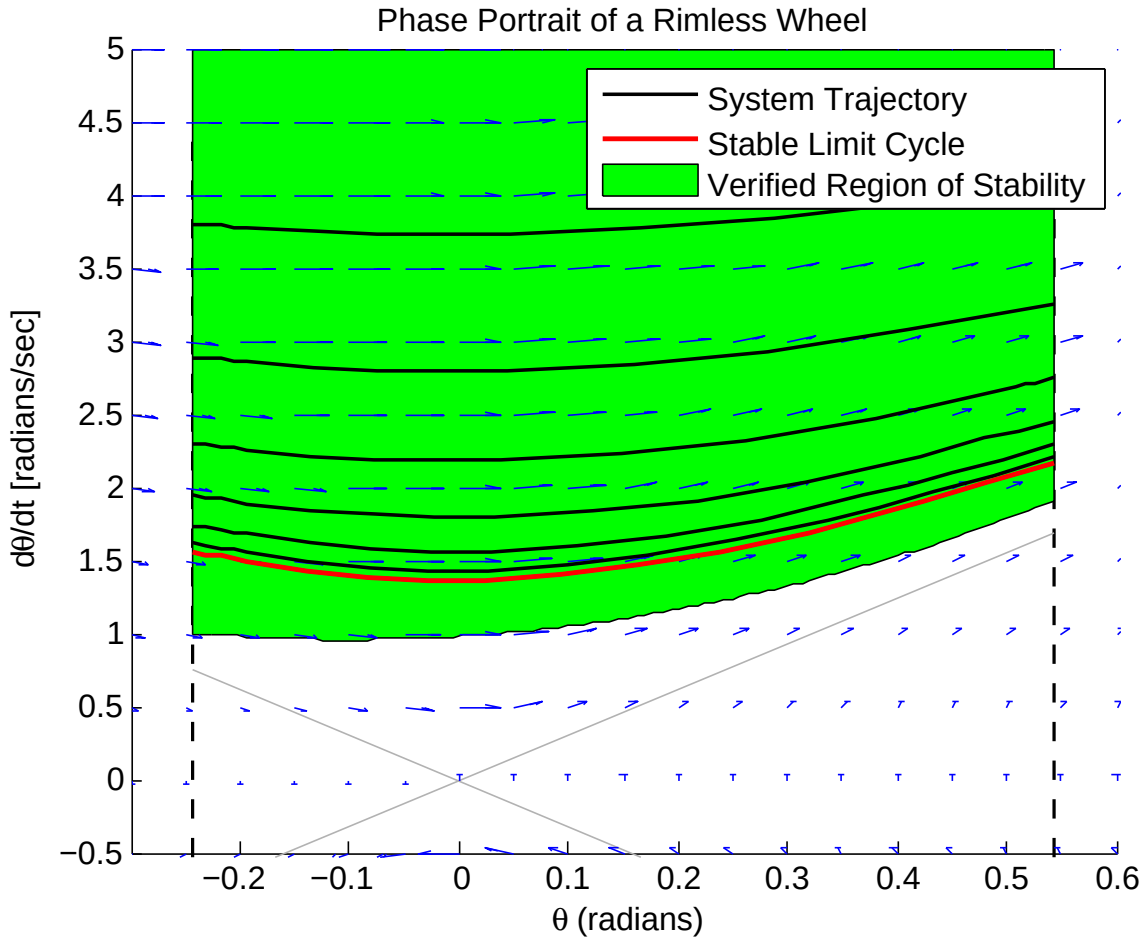

Figure 3.7 – Verified region of transverse contraction for Rimless Wheel

that the transverse contraction framework decouples the question of convergence from knowledge of a particular solution. This opens doors to robustness analysis when the exact location of the limit cycle is unknown due to uncertainty in the dynamics.

Chapter 4

Prescribed Co-ordinates for Simplified Stability Analysis of Nonlinear Hybrid Limit Cycles

While the theoretical results presented in the previous chapter enables stability analysis for nonlinear hybrid limit cycles, two problems remain for systems with higher dimensions:

1. For systems of high dimensionality, the resulting SOS conditions from the previous chapter can be numerically difficult to solve; and
2. Regions of stability for underactuated robots with non-trivial periodic solutions is naturally small and not easily defined in the full state space by Positivestellensatz.

In this chapter, we address these practical issues by constructing a new set of transverse co-ordinates, enabling simplified stability analysis on a set of reduced coordiantes.

This chapter includes results accepted and published in the 2017 IEEE International Conference on Robotics and Automation entitled "Invariant Funnels for Underactuated Dynamic Walking Robots: New Phase Variable and Experimental Validation"

([79]); as well as journal article entitled "Transverse Contracting Hybrid Systems and Robust Stability of Dynamic Walking Robots." ([78])

4.1 Introduction and Background

In recent years, computational methods using sum-of-squares representations and semidefinite programming [63] have been developed for region-of-attraction estimation for equilibria, e.g. [81], [76], and constructing feedback controllers, e.g. [52, 80]. Notable applications have included analysis of the falling-leaf mode of an F/A-18 fighter [17] and control design for a perching glider [60].

These computational methods are extended to analyse the stability of nonlinear hybrid limit cycles in [54, 57] by leveraging the concept of transverse dynamics, previously applied to *local* stability analysis and control of walking robots in [29, 55]. In [54, 57] a new coordinate system is defined on a family of transversal hypersurfaces which move about the limit cycle in accordance to a phase variable. Stability certificates can then be to be computed on the new transversal coordinates.

In this chapter, we demonstrate that for typical models of walking robots a significant simplification of the construction in [54, 57] is possible by use of a new phase variable. The relationship between this new phase variable and standard choice used in the *virtual constraints* methodology (e.g. in [55, 85]) is discussed in detail.

This chapter proceeds as follows. Section 4.2 introduces the class of problems that are considered in this paper and preliminaries. We explore and demonstrate the use of virtual constraints and the traditional choice of phase variable on a classic dynamic walking model – the compass gait walker – in Section 4.3. We then introduce a novel, optimal construction of the phase variable, with comparisons to the traditional choice. Using this new phase variable, we demonstrate ROA analysis in Section 4.4 with illustrative numerical results demonstrating the utility of our framework in Section 4.6.

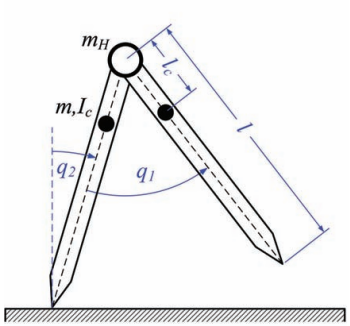

Figure 4.1 – The Compass Gait Walker, used as an example throughout this Chapter.

4.2 Problem Formulation and Preliminaries

Consider a hybrid system, with state space $x \in \mathbb{R}^n$ and continuous dynamics represented by

$$\dot{x} = f(x, u). \tag{4.1}$$

On a given switching surface $S^- \in \mathbb{R}^n$ the system (4.1) undergoes an instantaneous update

$$x^+ = g(x^-) \qquad x^- \in S^-. \tag{4.2}$$

Suppose $x^\star(\cdot)$ represents a periodic walking motion for the system, i.e., a non-trivial T-periodic trajectory satisfying (4.1), (4.2), with $u^\star(\cdot)$ the associated input trajectory.

The overall objective is twofold. First, we seek to compute an *invariant funnel* for periodic walking motion. That is, we seek to compute a region of state space $D \subset \mathbb{R}^n$ around $x^\star$, from which all solutions would remain in that region while maintaining forward motion. For the compass gait walker in Fig 4.1, forward motion is defined as positive angular velocity for q_2, thereby inducing forward movement of the hip.

Second, we seek to apply the contraction framework discussed in Chapter 3 to compute a *stability funnel* for the periodic walking motion. That is, we seek to compute a region of state space $D \subset \mathbb{R}^n$ around $x^\star$, from which all solutions converge to a unique stable limit cycle.

Our approach is to first construct a set of transverse dynamics in regions around $x^\star(\cdot)$ as suggested in [54], which in turn enables:

1. the search for a Lyapunov function in the transverse dynamics to prove the invariance condition; and

2. the search for a contraction metric in the transverse dynamics to prove the stability condition.

For completeness, we now briefly restate the transverse coordinate construction from [54], highlighting improvements and simplifications made in this paper.

We define a smooth local change of coordinates $x \mapsto (\tau, x_\perp)$. At each point $t \in [0, T]$, we define a hyperplane $S(t)$, with $S(0) = S(T)$. These transversal surfaces are defined by

$$S(\tau) = \{y \in \mathbf{R}^n : z(\tau)^T (y - x^\star(\tau)) = 0\} \tag{4.3}$$

where $z : [0, T] \to \mathbb{R}^n$ is a vector function defining the normal vector of each surface and would be optimised in Section 4.3. $S(\tau)$ is a valid transversal surface iff $z(\tau)^T f(x^\star(\tau)) > 0, \forall \tau \in [0, \tau]$.

Given a point x nearby $x^\star(\cdot)$, the phase variable $\tau \in [0, T)$ represents which of these transversal surfaces $S(\tau)$ the current state x inhabits; the vector $x_\perp \in \mathbb{R}^{n-1}$ is the transversal state representing the location of x within the hyperplane $S(\tau)$, with $x_\perp = 0$ implying that $x = x^\star(\tau)$. More precisely,

$$x_\perp = \Pi(\tau)(x - x^\star(\tau)) \tag{4.4}$$

where $\Pi(\tau)$ is a projection operator constructed from $z(\tau)$, as will be discussed in Section 4.4.

The dynamics of the system in these new coordinates can be expressed as [54, Theorem 1] :

$$\dot{\tau} = \frac{z(\tau)^T f(x^\star(\tau) + \Pi(\tau)^T x_\perp)}{z(\tau)^T f(x^\star(\tau)) - \frac{\partial z(\tau)}{\partial \tau}^T \Pi(\tau)^T x_\perp} =: \frac{n(x_\perp, \tau)}{d(x_\perp, \tau)} \tag{4.5}$$

$$\dot{x}_\perp = \dot{\tau} \left[\frac{d}{d\tau}\Pi(\tau)\right] \Pi(\tau)^T x_\perp + \Pi(\tau) f\Big(x^*(\tau) \tag{4.6}$$

$$+ \Pi(\tau)^T x_\perp \Big) - \Pi(\tau) f\left(x^\star(\tau)\right) \dot{\tau}.$$

The construction of $z(\tau)$ and $\Pi(\tau)$ in this paper has been significantly simplified compared to that proposed in [54]. We achieve this by making three assumptions about the properties of the system in consideration: its dynamics; its switching surface S^-; and its target trajectory $x^\star$.

First, we assume that the state space can be represented in terms of the configuration space and its velocities $x = \left[q^T, \dot{q}^T\right]^T$; and that its dynamics can be written in the form $f = \left[\dot{q}^T, \hat{f}(q, \dot{q}, u)^T\right]^T$.

This assumption is satisfied for mechanical systems written in Euler-Lagrange form:

$$M(q)\ddot{q} + C(q, \dot{q})\dot{q} + G(q) = B(q)u. \tag{4.7}$$

or equivalently represented in n-dimensional state space with $x = [q_1, q_2, \dot{q}_1, \dot{q}_2]^T$ and,

$$\hat{f}(q, \dot{q}, u) = M^{-1}(q)[-C(q, \dot{q})\dot{q} - G(q) + B(q)u]$$

Second, we assume that the switching surface S^- is a hyperplane which can be entirely represented in terms of the configuration space q. That is, it can be defined as $a^T q + b = 0$ for some vector a of length $n/2$ and some scalar b.

Third, we assume that the periodic walking motion $x^\star(\cdot)$ can be represented by a monotonic phase variable dependent only on q. In particular for our system, this can be guaranteed if $x^\star(\cdot)$ was designed by a set of virtual constraints. In a virtual constraint, a monotonic phase variable $\tau(q)$ is used to parameterize the motion of the robot within a step. Traditionally, $\tau(q)$ would be synthesized from angular measurements, an inclinometer, or some combination of these. We represent the virtual constraint like so:

$$q := \phi(\tau) = [\phi_1(\tau), \cdots, \phi_{n/2}(\tau)]^T. \tag{4.8}$$

4.3 Virtual Constraints and Phase Variable Selection

In this section, we first illustrate the use of a traditional choice of phase variable in a virtual constraint, and its incompatibility with regional analysis. We then provide a simplified and novel construction of a phase variable which addresses these issues and significantly simplifies the construction of transverse dynamics in Eqs. (4.5)-(4.6).

Throughout the remainder of this paper, we will illustrate our method with our hardware platform, modelled after the classic underactuated compass gait walker as shown in Figure 4.1. Here, q_1 is referred to as the 'swing leg' while q_2 is referred to as the 'stance leg'. The hybrid dynamics of the walker can be found in the Appendix. Note that we adopt the convention of positive angle as clockwise, hence the stance leg angle, θ_{st} is monotonically *increasing* through a footstep.

Foot impact occurs when the swing leg hits the ground. Hence, the switching surface S^- as defined in the discrete update Eq. (4.2) is

$$S^- = \{x \in \mathbb{R}^n : q_1 = 2q_2\}. \tag{4.9}$$

With appropriate parameter configurations and control law, the compass gait walker can follow a designated limit cycle trajectory. Figure 4.2 plots the 4-dimensional state space of one such limit cycle as tested in the hardware, with the stance leg dynamics superimposed with the swing leg dynamics. The green circles show the starting points for both the stance leg and the swing leg immediately after impact; while the magenta crosses illustrate the impact point.

4.3.1 The Traditional Phase Variable on the Compass Gait

Typically in virtual constraint design for the compass gait walker [85], it is common to select the stance leg angle, θ_{st}, as the phase variable, i.e.,

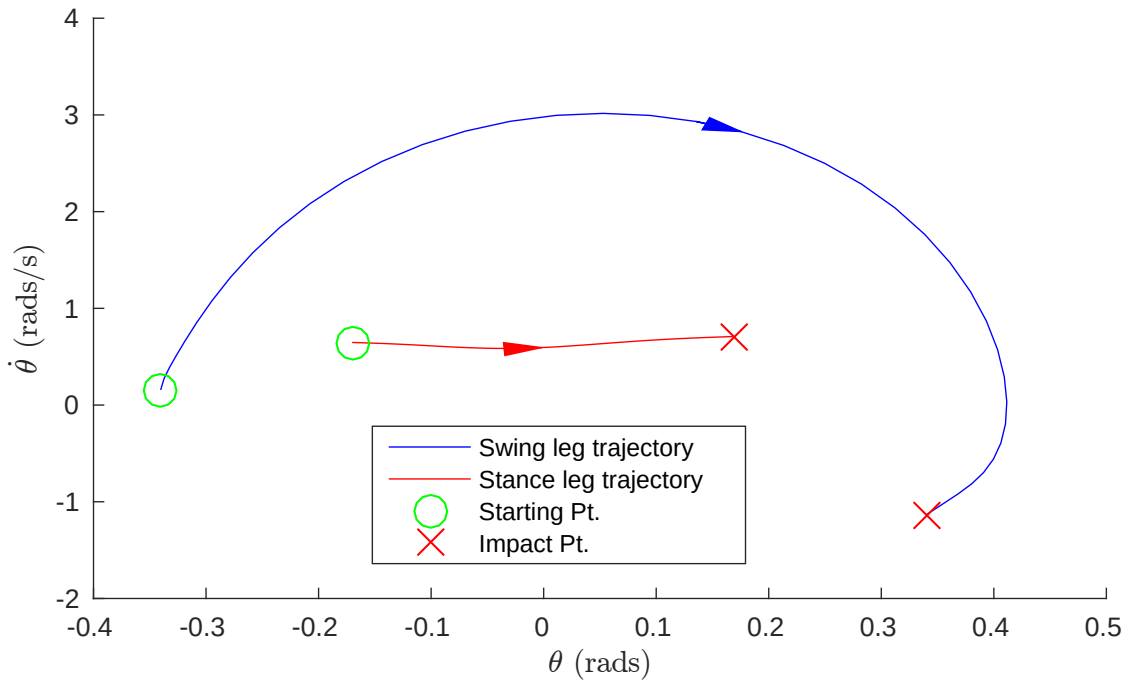

Figure 4.2 – The phase portrait for the compass gait hardware in limit cycle motion.

$$\tau(q) = \theta_{st}.$$

In Figure 4.3, we highlight the use of this traditional choice of phase variable and the difficulties this presents in transverse stability analysis. The black solid line shows the same trajectory represented in Figure 4.2, with the black arrow indicating the direction of the dynamics. Red arrows drawn throughout the trajectory indicate the vector $z(\tau)$ which represents the direction in which the phase variable advances at that point.

In this case, the phase variable only advances in the direction of the stance leg angle throughout the cycle and hence θ_{st} is the only component in these vectors, i.e., $z = [0, 1, 0, 0]^T$. Note that monotonicity of the phase variable is equivalent to the red arrows forming acute angles with the direction of the black trajectory or $z^T\dot{x} > 0$ – i.e., the flow of the trajectory is constantly advancing the phase variable.

As per Eq. (4.3), the vertical blue lines in Figure 4.3 are surfaces transverse to $z(\tau)$. These transversal surfaces represent the set of states that can be associated with a particular phase value. For example, the leftmost transversal surface here represents the set of possible states that can be associated with $\tau \approx -0.17$ rads.

For simplicity, it is often assumed that switching occurs at a predesignated phase θ_{st}^d (see, e.g., [85, pp. 165-166]). This assumes the switching surface S^- to take the form,

$$S^- = \{x \in \mathbb{R}^n : \theta_{st} = \theta_{st}^d\}. \tag{4.10}$$

In Figure 4.3, this switching surface is equivalent to the leftmost transversal surface. However, this could only occur if one of the following two conditions hold true.

Condition 4.1 (Impact point in state space)**.** The point of impact always precisely equals that of on the nominal trajectory. This essentially assumes a finite-time controller guarantees the walker reach and remain on the target trajectory within one foot step.

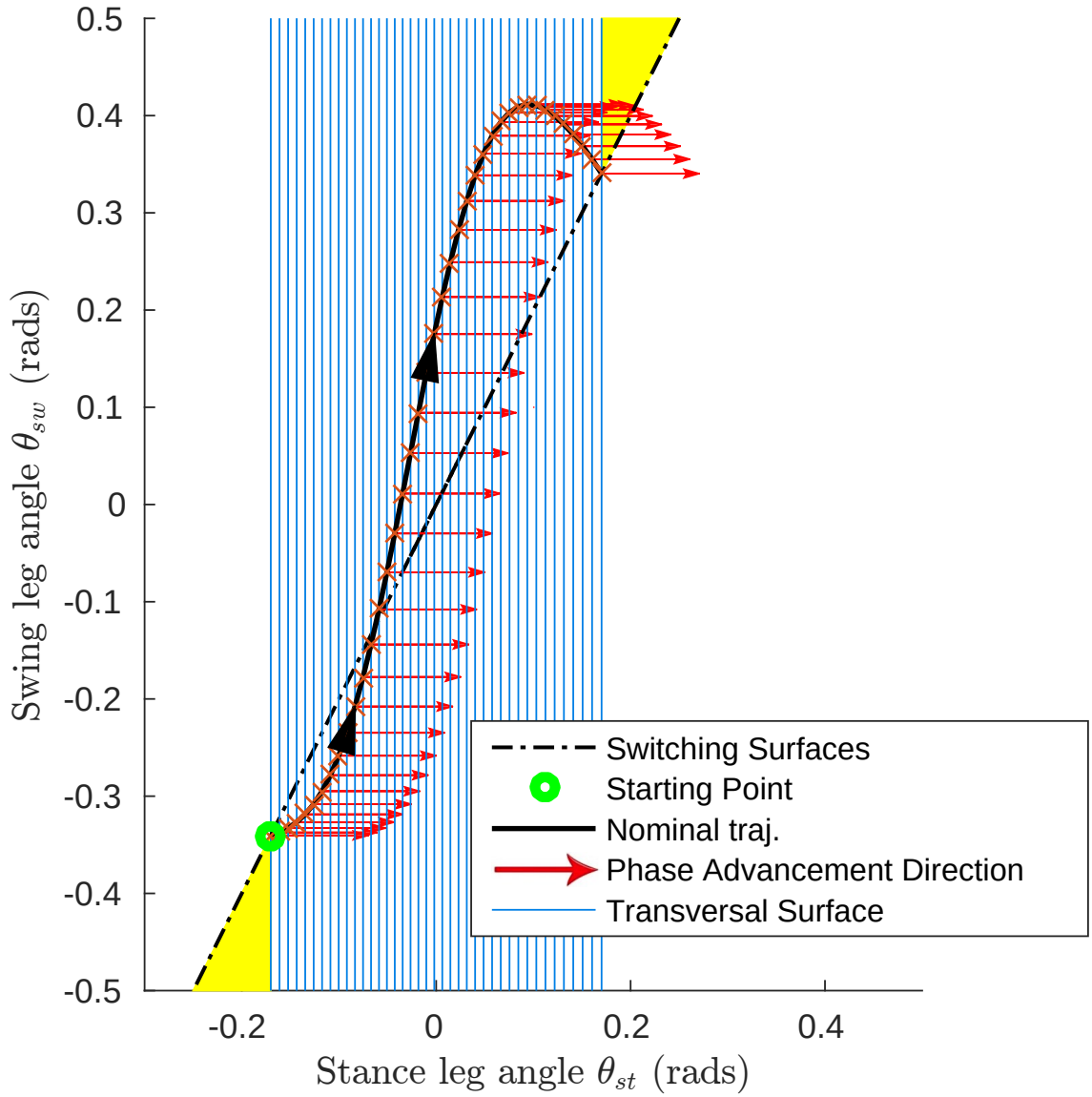

Figure 4.3 – Illustration of traditional phase variable for the compass gait walker – θ_{st}. Red arrows indicates the direction of $z(\tau)$ i.e., the direction in which the phase variable is increasing; blue lines indicate the transversal surfaces – the set of possible states corresponding to a particular phase value.

Condition 4.2 (Impact trigger)**.** The walker has the ability to artificially trigger impact at the instant the designated final phase variable (θ_{st}^d) is reached.

Both Conditions 4.1 and 4.2 are arguably difficult to realise precisely with physical hardware. Indeed, if either conditions were not perfectly followed, impact would naturally occur when Equation (4.9) is satisfied, which is illustrated as black dotted line in Figure 4.3.

Given the discrepancy between the switching surface that this traditional choice of phase variable assumes – Eq. (4.10) – and the "natural interpretation" of the switching surface – Eq. (4.9) – the yellow shaded areas in Figure 4.3 mark problematic regions for analysis. In these regions – which occur when the Conditions 4.1 and 4.2 are not strictly met and the walker deviates from the nominal trajectory – the state would be undefined by this traditional phase variable. Therefore, any feedback controller expressed as a function of this phase variable would "run out of tape" in these shaded regions.

For transverse analysis, the shaded regions are undefined as they are not associated with any phase variable. Intuitively, if the leftmost and rightmost blue line aligned with the dotted line, the yellow shaded regions would disappear. Figure 4.4 shows the result of such arrangement, which will now be discussed.

4.3.2 Construction of a Novel Phase Variable

We now propose the construction of a new phase variable which aligns with the switching surface, overcoming the issues described in the previous section, and yet is significantly simpler than the construction proposed in [54].

Geometrically from Figure 4.4, to align the transversal surfaces with the switching surface in Eq. (4.9) is equivalent to enforcing the direction of the two outermost red arrows being $[-1, 2, 0, 0]^T$. To simplify derivations of the transverse dynamics, we

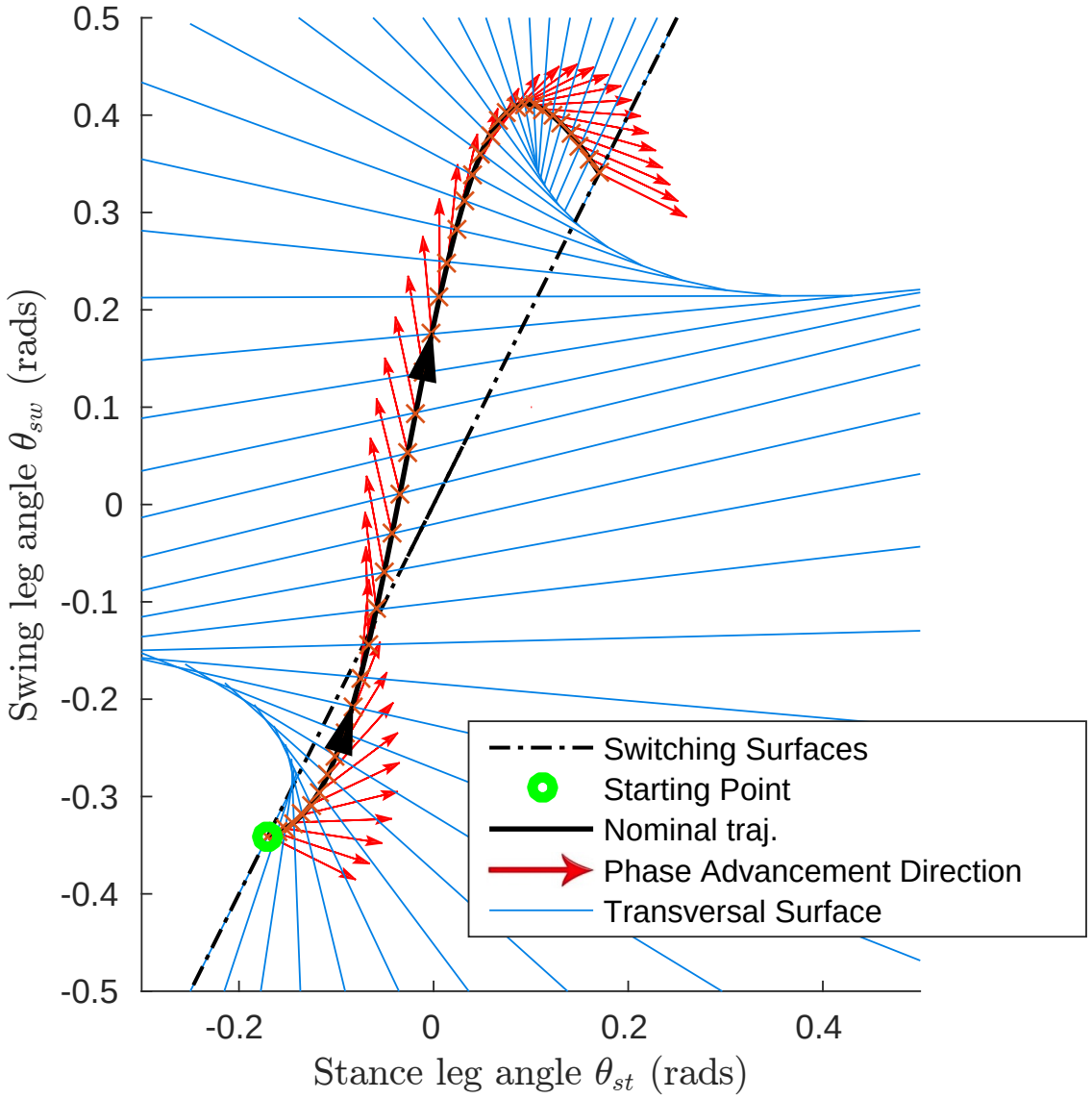

Figure 4.4 – Illustration of a new phase variable for the compass gait walker - a combination of both stance and swing angle. Red arrows indicates the direction $z(\tau)$, i.e. the direction in which the phase variable is increasing.

enforce $|z| = 1$, hence this condition becomes:

$$z(x^+) = z(x^-) = \left[\frac{-1}{\sqrt{5}}, \frac{2}{\sqrt{5}}, 0, 0\right]^T. \tag{4.11}$$

For the compass-gait walker, we propose a simple parametrization of z in terms of the angle of the red arrows in Fig 4.4, ψ:

$$z(\psi(\tau)) = [\cos(\psi(\tau)), \sin(\psi(\tau)), 0, 0]^T, \tag{4.12}$$

with

$$\frac{\partial z(\tau)}{\partial \tau} = [-\sin(\psi)\dot{\psi}, \cos(\psi)\dot{\psi}, 0, 0]^T.$$

Computations can be further simplified by parametrizing $\psi(\tau)$ as a Bezier polynomial, which allows the enforcement of (4.11) by simply fixing the first and last coefficients.

In addition to aligning with the switching surface, $z(\tau)$ must ensure that the transformation to transverse dynamics is well-posed. From Equation (4.5), it is apparent that the transformation $x \mapsto (x_\perp, \tau)$ is ill-defined when the denominator of $\dot{\tau}$, or $d(x_\perp, \tau)$, is zero, i.e.,

$$z(\tau)^T f(x^\star(\tau), u^\star(\tau)) - \frac{\partial z(\tau)}{\partial \tau}^T \Pi(\tau)^T x_\perp = 0. \tag{4.13}$$

As derived in [54], the smallest transversal $x_\perp^\dagger$ for which (4.13) is true has norm

$$|x_\perp^\dagger(\tau)| = \frac{|z(\tau)^T f(x^\star(\tau), u^\star(\tau)))|}{|\frac{\partial z(\tau)}{\partial \tau}|}.$$

In this paper, we modify the method of [54] by considering the distance from $x_\perp^\dagger$ to its projection on to the line spanned by $f(x^\star(\tau), u^\star)$, as illustrated in Fig. 4.5. The resulting distance d approximates the distance from $x_\perp^\dagger$ to the trajectory, and is computed like so:

$$d = |x_\perp^\dagger(\tau)| \cos(\alpha) = \frac{|z(\tau)^T f(x^\star(\tau), u^\star(\tau))|}{|\frac{\partial z(\tau)}{\partial \tau}|} z(\tau)^T \bar{f}(\tau), \tag{4.14}$$

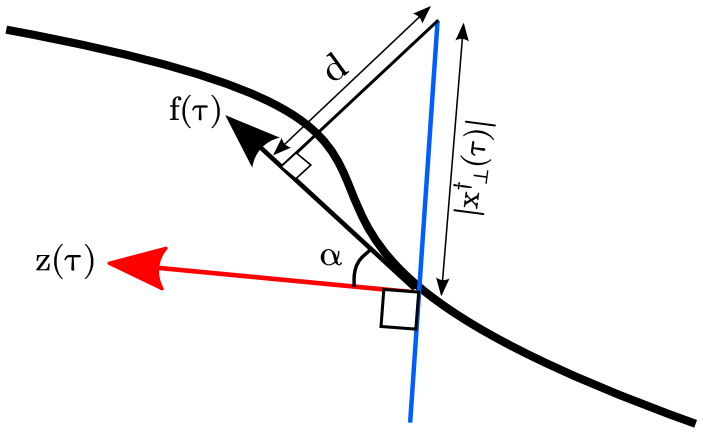

Figure 4.5 – Illustration of the distance, d, to be optimized in order to maximise the region that can be represented by the transverse dynamics.

where $\bar{f}(\tau) = \frac{f(x^\star(\tau),u^\star(\tau))}{|f(x^\star(\tau),u^\star(\tau))|}$ and α is the angle between $z(\tau)$ and $f(x^\star(\tau), u^\star(\tau))$.

However, note that the denominator in (4.14) contains $\frac{\partial z(\tau)}{\partial \tau}$. The optimum solution may contain constant $z(\tau)$ for some interval of τ; thereby causing (4.14) to go to infinity. Hence, instead of maximising (4.14), we find it is better numerically posed to optimise for z by minimizing the inverse of (4.14):

$$\begin{aligned} & \arg\min_{z(\tau)} \left(\int_0^T \frac{|\frac{\partial z(\tau)}{\partial \tau}|^p}{|z(\tau)^T f(x^\star(\tau), u^\star(\tau)) z^T \bar{f}|^p} d\tau \right)^{1/p} \\ s.t. \quad & z(x^+) = z(x^-) = \left[\frac{-1}{\sqrt{5}}, \frac{2}{\sqrt{5}}, 0, 0 \right]^T \\ & z(\tau)^T f(x^\star(\tau), u^\star(\tau)) > \delta. \end{aligned} \tag{4.15}$$

The decision variables for the optimization are the coefficients of the Bezier polynomial defining ψ in (4.12). The authors have had success setting $p = 100$ and $\delta = 0.06$. With a desktop computer equipped with a 3.4 GHz Intel i7 and 24 GB of RAM, this can be solved within 5 seconds with ψ parameterised as a 5^{th} order Bezier polynomial, with results shown in Fig 4.4.

This construction is simpler than that in [54] since z only has non-zero entries in θ_{sw} and θ_{st}, the optimization for $z(\tau)$ can be directly computed from any virtual constraint definition in the form of (4.8).

4.4 Transverse analysis with a geometric phase variable via sums-of-squares programming

With the new simplified phase variable derived in Section 4.3, we now demonstrate transverse stability analysis leading to an explicit region of stability in the full state space of the compass gait walker. Our approach proceeds as follows:

1. Compute the transverse dynamics using the simplified phase variable, as discussed in Section 4.4.1
2. Design a stabilizing controller and derive an initial seed for the Lyapunov function or contraction metric, as discussed in Section 4.4.2;
3. Define τ-varying regions around $x^\star(\cdot)$ for which the invariance or stability conditions will be checked. Then, leverage the S-procedure and sum-of-squares optimization to iteratively maximise:
   (a) the invariance region, to be discussed in Section 4.4.3; or
   (b) the contracting region, to be discussed in Section 4.4.4.

We now explore each of these steps, highlighting improvements and simplifications made in our approach over that reported in [54].

4.4.1 Transverse Dynamics Computation

The new simplified phase variable, as defined by $z(\tau)$ in (4.12), enables significantly simpler computation for the transverse dynamics. For the compass gait, the projection

operator, i.e. Π in (4.4), and its derivative can now be analytically computed:

$$\Pi(\tau) = \begin{bmatrix} -\sin(\psi(\tau)) & \cos(\psi(\tau)) & 0 & 0 \\ 0 & 0 & 1 & 0 \\ 0 & 0 & 0 & 1 \end{bmatrix}$$

$$\frac{d}{d\tau}\Pi(\tau) = \begin{bmatrix} -\cos(\psi(\tau))\frac{d\psi}{d\tau} & -\sin(\psi(\tau))\frac{d\psi}{d\tau} & 0 & 0 \\ 0 & 0 & 0 & 0 \\ 0 & 0 & 0 & 0 \end{bmatrix}.$$

Note that the analytical construction of Π and $\frac{d}{d\tau}\Pi$ and the resulting sparsity of these variables significantly simplifies computations compared with methods suggested in [54]. Specifically, since $\left[\frac{d}{d\tau}\Pi(\tau)\right]\Pi(\tau)^T = 0$, the first term of (4.6) goes to zero, resulting in vastly simpler transverse dynamics:

$$\dot{x}_\perp = \Pi(\tau)(f_\perp(\tau) - f_\star(\tau)\dot{\tau}) \tag{4.16}$$

where $f_\perp(\tau) = f\Big(x^*(\tau) + \Pi(\tau)^T x_\perp, u(x_\perp, \tau)\Big)$ and $f_\star(\tau) = f(x^\star(\tau), u^\star(\tau))$.

The switching condition in the new coordinates is given by:

$$\begin{aligned} x_\perp^+ = g_\perp(x_\perp^-) &= \Pi(\tau^+)[x^+ - x^{\star+}] \\ &= \Pi(\tau^+)\Big[g\big(\Pi^T(\tau^-)x_\perp^- + x^{\star-}\big) - x^{\star+}\Big] \end{aligned} \tag{4.17}$$

Using the transverse dynamics in (4.16), we can now construct Lyapunov functions which prove orbital stability by showing $x_\perp \to 0$ as $t \to \infty$.

4.4.2 Stabilizing Controller and Initial Seed for the Lyapunov Function

A natural candidate for a stabilizing controller can be obtained via the solution of the transverse-jump-Riccati equation.

$$\begin{aligned} -\dot{P} &= A^T P + PA - PB_\perp R^{-1} B_\perp^T P + Q_\perp, && t \neq t_i \\ P(\tau_i^-) &= A_d(\tau_i)^T P(\tau_i^+) A_d(\tau_i) + Q_i, && t = t_i \end{aligned}$$

where $R, Q, Q_i > 0$;

$$B_\perp = \Pi(\tau)\frac{\partial f(x^\star(\tau), u^\star(\tau))}{\partial u} - \Pi(\tau) f(x^\star(\tau), u^\star(\tau))\frac{\partial \dot{\tau}}{\partial u};$$

and A is the linearization of $\dot{x}_\perp$ w.r.t. $x_\perp$. Given the simplification of the transverse dynamics in (4.16), a simplified expression of A over [54, Eq. (18)] is:

$$A(t) = \Pi(t)\left(\frac{\partial f(x^\star(t), u^\star(t))}{\partial x}\Pi(t)^T - f(x^\star(t), u^\star(t))\left.\frac{\partial \dot{\tau}}{\partial x_\perp}\right|_{x_\perp=0}\right).$$

The solution of the transverse-jump-Riccati equation forms a locally stabilizing, phase-varying feedback controller:

$$u(\tau, x_\perp) = u^\star(\tau) - R^{-1} B_\perp(\tau)^T P(\tau) x_\perp. \tag{4.18}$$

Using the transverse-LQR controller in (4.18), we yield the close loop system which, for brevity, we will hereafter refer to as follows:

$$f_{cl}(x) = f(x, u(\tau, x_\perp))$$

where $u(\tau, x_\perp)$ is defined in (4.18).

The transverse-jump-Riccati solution also forms a locally valid Lyapunov function for the closed-loop system, $V(x_\perp, \tau)$ for a small region around $x^\star$ like so

$$V(x_\perp, \tau) = x_\perp^T P(\tau) x_\perp. \tag{4.19}$$

we now demonstrate verification of the stability of the closed loop system by:

(i) constructing invariant funnels using Lyapunov functions in Section 4.4.3; and

(ii) constructing stability funnels using contraction metrics in Section 4.4.4.

4.4.3 Constructing Invariant Funnels via Lyapunov Function

To construct the invariant funnels, we seek to compute a the τ-varying sets $D(\tau)$ such that for some $t_0 \in [0, \infty)$,

$$x_\perp(\tau(t_0)) \in D(\tau(t_0)) \implies x_\perp(\tau(t)) \in D(\tau(t)) \quad \forall t \in [t_0, \infty).$$

We describe this invariant funnel as a τ-varying sub-level set of a function $\check{V}(x_\perp, \tau)$:

$$D(\tau) = \{x_\perp \mid \check{V}(x_\perp, \tau) < \rho(\tau)\}. \tag{4.20}$$

In the continuous phase of the system, we require the invariance condition on the boundary of the funnel:

$$\check{V}(x_\perp, \tau) = \rho(\tau) \implies \dot{\check{V}}(x_\perp, \tau) < \dot{\rho}(\tau). \tag{4.21}$$

To allow the condition $\dot{\check{V}} < \dot{\rho}$ to be verified via sums-of-squares (SOS) programming, we multiply $\dot{\check{V}}$ through by $d(x_\perp, \tau)$, with $d(x_\perp, \tau)$ defined in Eq. (4.5). This results in an equivalent Lyapunov condition in (4.22), as shown below.

$$DV := \frac{\partial \check{V}}{\partial \tau} n(x_\perp, \tau) + \frac{\partial \check{V}}{\partial x_\perp} \Big\{ d(x_\perp, \tau)\Pi(\tau) f_{cl}\left(x^*(\tau) + \Pi(\tau)^T x_\perp\right) - \Pi(\tau) f_{cl}\left(x^\star(\tau)\right) n(x_\perp, \tau) \Big\} \leq d(x_\perp, \tau)\dot{\rho} \tag{4.22}$$

We also approximated the closed-loop dynamics with a third-order Taylor series expansion. We will discuss the ramification of the Taylor approximation in Section 4.6.

In the discrete phase of the system, the condition to be verified at the time of switching is:

$$\check{V}(x_\perp^+, \tau^+) \leq \check{V}(x_\perp^-, \tau^-). \tag{4.23}$$

Applying the transverse transformation, this becomes:

$$\check{V}\Bigg(\Pi(\tau_i^+)\Big[g_i\left(x^\star(\tau_i) + \Pi(\tau_i^-)^T x_\perp\right) - x^\star(\tau_i^+)\Big], \tau_i^+ \Bigg) - \check{V}(x_\perp, \tau_i^-) \leq 0$$

Similar to [57], we verify the continuous (4.21) and discrete (4.23) invariance conditions on the boundary of the invariant funnel D by sampling $N = 40$ values of τ along the limit cycle trajectory.

In theory, we can parameterise the Lyapunov function $\check{V}$ by polynomial in $x_\perp$ and τ. However, this often leads to numerical problems in the resulting SOS program due to the high number of decision variables. We therefore parameterise $\check{V}$ by incorporating a τ-varying matrix Φ to the 'initial seed' of the Lyapunov function in (4.19), like so:

$$\check{V} = x_\perp^T (P(\tau) + \Phi(\tau)) x_\perp.$$

We can now maximise the invariant funnel for the limit cycle by using the integral of ρ as a surrogate for maximising the volume of the regions. Hence, the verification using SOS, with the S-procedure and Lagrange multipliers $l_1(x_\perp, \tau)$ and $l_2(x_\perp, \tau)$ is:

$$\max_{\check{V}, \rho(\tau), l_1, l_2} \int_0^T \rho(\tau) d\tau \tag{4.24}$$

subject to

$$-DV(x_\perp, \tau) - d(x_\perp, \tau)\dot{\rho}$$
$$-l_1(x_\perp)(\rho - V(x_\perp, \tau)) \in SoS, \tag{4.25}$$
$$d(x_\perp, \tau) - l_2(x_\perp)(\rho - V(x_\perp, \tau)) \in SoS, \tag{4.26}$$
$$\check{V}(x_\perp^-, \tau^-) - \check{V}(x_\perp^+, \tau^+) \in SoS, \tag{4.27}$$
$$V_{guess}(\Sigma_j e_j, \tau) - \check{V}(\Sigma_j e_j) > 0, \tag{4.28}$$
$$l_2 \in SoS. \tag{4.29}$$

Similar to [52], (4.28), is a constraint which prevents a large ρ to be returned simply by the scaling of Φ; where e_j is the j-th standard basis vector for the state space $\mathbb{R}^n$, and V_{guess} is defined by (4.19).

As can be seen, the above optimisation program is non-convex as the conditions are bilinear in the decision variables. Hence, we perform a bilinear search for the funnel as shown in Algorithm 1. In our approach, we find that formulating ρ as a Chebyshev polynomial reduces numerical problems in the resulting SOS program, when compared with parameterizing it as a piecewise polynomial or with a monomial basis.

4.4.4 Constructing Stability Funnels via Contraction Metric

In Chapter 3, orthogonality has been defined via the Riemannian metric M. Such approach combines the search for both the stability certificate and the orthogonality definition into one convex problem – the search for M. However, even with current

Algorithm 1 Maximising Invariant Funnel Volume

Initialise: set $\Phi = 0$; and set ρ as the maximal constant (via bisection search) that satisfies (4.21) and (4.23) throughout the limit cycle trajectory;
converged = 0;
previousObj = 0;
while not converged **do**
    Multiplier-step: Fix ρ and solve feasibility problem to find Lagrange multipliers l_1, l_2 satisfying (4.25) to (4.29).
    ρ**-step**: Fix the l_1, l_2 and maximise the objective $\int \rho \, d\tau$ in (4.24) satisfying (4.25) to (4.29).
    if $\frac{\int \rho \, d\tau - \text{previousObj}}{\text{previousObj}} < \epsilon$ **then**
        converged = 1;
    end if
    previousObj = $\int \rho \, d\tau$
    compare integral with previous; save current integral
end while

state-of-the-art numerical solver, the authors found that the resulting search for such M may be intractable for some higher dimensional systems.

We now demonstrate that the enforcement for the orthogonality condition can be performed separately by using the explicit transverse coordinates construction outlined in Section 4.4.1. This transformation enables the direct search for a reduced $(n-1)$-dimensional metric, $M_\perp$, significantly simplifying the resulting numerical search for a metric. The obvious trade-off is the need to construct the new set of transverse coordinates outlined in Section 4.4.1.

Theorem 4.1 (Contraction in reduced transverse coordinates)**.** Suppose we can define a phase variable τ which is monotonically increasing along the cycle: i.e., with $\frac{\partial \tau}{\partial x} =: z(\tau)$, $z(\tau)^T f(x(\tau)) > 0$. We construct a new set of coordinates $x_\perp$ orthogonal to $z(\tau)$. Further, during switching, $z(\tau)$ aligns with the normal of the switching surface S_i in (3.2).

If there exists a contraction metric in $x_\perp$, that is, firstly during the continuous phase, there exists $M_\perp$ satisfying

$$\frac{\partial f_\perp}{\partial x_\perp}^T M_\perp(x) + M_\perp(x)\frac{\partial f_\perp}{\partial x_\perp} + \dot{M}_\perp(x) < 0. \tag{4.30}$$

and secondly during the discrete phase,

$$\frac{\partial g_\perp}{\partial x_\perp}^T M_\perp^+ \frac{\partial g_\perp}{\partial x_\perp} - M_\perp^- < 0 \tag{4.31}$$

then the system is transverse contracting and there exists a stable limit cycle.

Proof. Construct a set of bases $e_1, ..., e_n$ using the new coordinates, where $e_1 =: z(\tau)$ and $e_2, ...e_n$ are transverse to $z(\tau)$. Proof of stable limit cycle follows from construction in Lemma 3.2 with B_H constructed from $e_2...e_n$ which are contracting. □

Remark 4.1 (Existence of angular variable)**.** Existence of τ is closely related to the study of foliation of codimension one. From [15, Theorem 4.1], if there exists an asymptotically stable periodic orbit, then there exists a smooth, diffeomorphic transformation which admits τ, an angular variable.

Using the construction of the transverse dynamics in (4.16), (4.17), stability can now be proved by searching for a contraction metric $M_\perp$ which satisfies (4.30), (4.31). As mentioned in Section 4.4.2, to attain an initial seed for the contraction metric $M_\perp$ and a locally optimal feedback controller, it is common to solve the jump-Riccati equation associated with the linearization of the transverse dynamics like so:

$$-\dot{P} = A_\perp^T P + P A_\perp - P B_\perp R^{-1} B_\perp^T P + Q_\perp, \qquad t \neq t_i \tag{4.32a}$$

$$P(\tau_i^-) = A_d(\tau_i)^T P(\tau_i^+) A_d(\tau_i) + Q_i, \qquad t = t_i \tag{4.32b}$$

where $R, Q, Q_i > 0$;

$$B_\perp = \Pi(\tau)\frac{\partial f(x^\star(\tau), u^\star(\tau))}{\partial u} - \Pi(\tau) f(x^\star(\tau), u^\star(\tau))\frac{\partial \dot{\tau}}{\partial u};$$

and $A_\perp$ is the linearization of $\dot{x}_\perp$ in (4.6) w.r.t. $x_\perp$; A_d is the linearization of $x_\perp^+$ in (4.17) w.r.t. $x_\perp$. The feedback law is given by:

$$u(\tau, x_\perp) = u^\star(\tau) - R^{-1} B_\perp(\tau)^T P(\tau) x_\perp. \tag{4.33}$$

We seek to verify the contraction region of the closed loop system, of which $P(\tau)$ is a locally valid contraction metric around $x_\perp = 0$. In theory, one can directly search for the metric $M_\perp$ parameterizing it as a polynomial in $x_\perp$ and τ. However, this often leads to numerical problems in the resulting SOS program due to the high number of decision variables. Therefore, we use the solution of the jump-Riccati equation, $P(\tau)$, as a valid initial seed for contraction metric in some small region satisfying for some small ρ_{init}:

$$V_{init}(x_\perp, \tau) := \frac{x_\perp^T P(\tau) x_\perp}{\rho_{init}} < 1. \tag{4.34}$$

Using this initial seed, extra flexibility for the contraction metric can be attained by

adding a τ-varying matrix, $\Phi(\tau)$ to a new metric, $M_\perp$ like so:

$$M_\perp(\tau) = \frac{P(\tau)}{\rho_{init}} + \Phi(\tau) \tag{4.35}$$

With $M_\perp$ the contraction condition becomes

$$\left(\frac{dP}{d\tau}\frac{1}{\rho_{init}} + \frac{d\Phi}{d\tau}\right)\dot{\tau} + \frac{\partial f_\perp}{\partial x_\perp}^T M_\perp + M_\perp \frac{\partial f_\perp}{\partial x_\perp} < 0. \tag{4.36}$$

Suppose now $\dot{\tau} = \frac{n(x_\perp,\tau)}{d(x_\perp,\tau)}$, we multiply through above by $d(x_\perp,\tau)$ to yield (4.37).

$$J := n(x_\perp,\tau)\left(\frac{dP}{d\tau}\frac{1}{\rho_{init}} + \frac{d\Phi}{d\tau}\right) + d(x_\perp,\tau)\left[\frac{\partial f_\perp}{\partial x_\perp}^T (P(\tau)+\Phi(\tau)) + (P(\tau)+\Phi(\tau))\frac{\partial f_\perp}{\partial x_\perp}\right] < 0 \tag{4.37}$$

We verify the contraction criteria in a τ-varying ellipsoidal region, i.e., a tubular region around $x^\star$ in the full state-space:

$$V(x_\perp,\tau) := x_\perp^T M_\perp(\tau) x_\perp < \rho \tag{4.38}$$

We can now maximise the contraction region for the limit cycle by using the value of ρ as a surrogate for maximising the volume of the regions. Hence, the verification using SOS, with Positivestellansatz [63] and Lagrange multipliers l is:

$$\max_{\Phi(\tau),\rho,l_1,l_2} \rho \tag{4.39}$$

subject to

$$-J(x_\perp,\tau) - l_1(x_\perp)(\rho - V(x_\perp,\tau)) \in SoS, \tag{4.40}$$

$$d(x_\perp,\tau) - l_2(x_\perp)(\rho - V(x_\perp,\tau)) \in SoS, \tag{4.41}$$

$$M_\perp^- - \left(\frac{\partial g_\perp}{\partial x_\perp}^T M_\perp^+ \frac{\partial g_\perp}{\partial x_\perp}\right) \in SoS, \tag{4.42}$$

$$V_{init}(\Sigma_j e_j,\tau) - V(\Sigma_j e_j,\tau) > 0, \tag{4.43}$$

$$l_1, l_2 \in SoS. \tag{4.44}$$

Similar to [52], (4.43) is a constraint which prevents a large ρ to be returned simply by the scaling of Φ; where e_j is the j-th standard basis vector for the state space $\mathbb{R}^n$; and V_{init}, V are defined by (4.34) and (4.38) respectively.

As can be seen, the above optimisation program is non-convex as the conditions are bilinear in the decision variables. Hence, maximization of the contraction region can be done via a bilinear search as shown in Algorithm 2.

Algorithm 2 Maximising Contraction Funnel Volume

Initialise: set $\Phi = 0$; and set ρ_{init} as the maximal constant (via bisection search) that satisfies the contraction criteria throughout the limit cycle trajectory;
converged = 0;
previousObj = 0;
while not converged **do**
    Multiplier-step: Fix ρ and solve feasibility problem to find Lagrange multipliers l_1, l_2 satisfying (4.40) to (4.44).
    ρ**-step**: Fix the l_1, l_2 and maximise the objective ρ in (4.39) satisfying (4.40) to (4.44) over decision variables ρ, $\Phi(\tau)$.
    if $\frac{\rho - \text{previousObj}}{\text{previousObj}} <$ threshold **then**
        converged = 1;
    end if
    previousObj = ρ
end while

It is important to note that the formulation of the contraction metric in this section automatically guarantees strict forward invariance of the verified contraction region. This is because:

1. $x^\star(\tau)$, corresponding to $x_\perp(\tau) = 0$, is a valid trajectory of the system for all τ;
2. the metric $M_\perp$, as defined in (4.35), is independent of $x_\perp$ and therefore all geodesic distance between trajectories for a given τ is a straight line.

Therefore, the geodesic distance between $x^\star(\tau)$ and any trajectories in the contracting region defined by (4.38) would constantly decrease and therefore the region is also strictly forward invariant.

4.5 Maximising Robust Stability Regions

As discussed in Section 3.5, the contraction framework is especially suitable for uncertain systems where the limit cycle location changes with parametric uncertainty. This is because the framework eliminates the need for linearization or the need to know the exact location of the limit cycle, which often changes with uncertainty. We now demosntrate that using the results of Section 4.4.4 further simplifies such robustness analysis by enabling the search for stability certificate in the reduced transverse coordinates.

Consider the hybrid system with parametric uncertainty.

$$\dot{x} = f_\delta(x,\delta) = f_0(x) + \delta f_1(x) \qquad x \notin S_i^- \tag{4.45}$$

$$x^+ = g_\delta(x,\delta) = g_0(x) + \delta g_1(x) \qquad x \in S_i^- \tag{4.46}$$

Robustness to parametric uncertainty can be ascertained by searching for a new contraction metric which maximises the uncertainty intervals on the error. For symmetric bounds, this can be done by incorporating one Lagrange multiplier L as below.

$$J - L(\epsilon - \delta^T\delta) < 0 \tag{4.47}$$

where J is defined in (4.37), and $L > 0$. For asymmetric bounds, two Lagrange multipliers L_1, $L_2 > 0$ are required:

$$J - L_1(\delta - \epsilon_{min}) - L_2(\epsilon_{max} - \delta) < 0 \tag{4.48}$$

Incorporating Positivestellansatz conditions for the region, the SOS conditions for the robustness analysis becomes:

$$\max_{\Phi(\tau),L_1,L_2} \epsilon \tag{4.49}$$

subject to

$$-J(x_\perp,\tau) - L_1(\delta-\epsilon_{min}) - L_2(\epsilon_{max}-\delta) \\ -l_1(x_\perp)(\rho - V(x_\perp,\tau)) \in SoS, \tag{4.50}$$

$$d(x_\perp,\tau) - L_1(\delta-\epsilon_{min}) - L_2(\epsilon_{max}-\delta) \\ -l_2(x_\perp)(\rho - V(x_\perp,\tau)) \in SoS, \tag{4.51}$$

$$M_\perp^- - \left(\frac{\partial g_\perp}{\partial x_\perp}^T M_\perp^+ \frac{\partial g_\perp}{\partial x_\perp}\right) \in SoS, \tag{4.52}$$

$$L_1, L_2 \in SoS. \tag{4.53}$$

As can be seen, the above condition is bilinear in the decision variables L and ϵ. Similar to Algorithm 1, the bounds can be maximised using a bilinear search as shown in Algorithm 3.

Algorithm 3 Maximising Robust Contraction Bounds

```
Initialise: set Φ, ρ_init with optimized results from Algorithm 1;
converged = 0;
previousObj = 0;
while not converged do
    Multiplier-step: Fix ϵ and solve feasibility problem
     to find Lagrange multipliers L_1, L_2 satisfying (4.50)
     to (4.53).
    ϵ-step: Fix L_1, L_2 and maximise the objective
     ϵ in (4.49) satisfying (4.50) to (4.53).
    if (ϵ − previousObj)/previousObj < threshold then
        converged = 1;
    end if
    previousObj = ϵ
end while
```

In general, strict invariance is not automatically guaranteed by the contracting region when uncertainty is considered. This is because it can no longer be taken granted that $x^\star(\tau)$, or $x_\perp(\tau) = 0$ is necessarily a valid system trajectory for all τ under uncertainty.

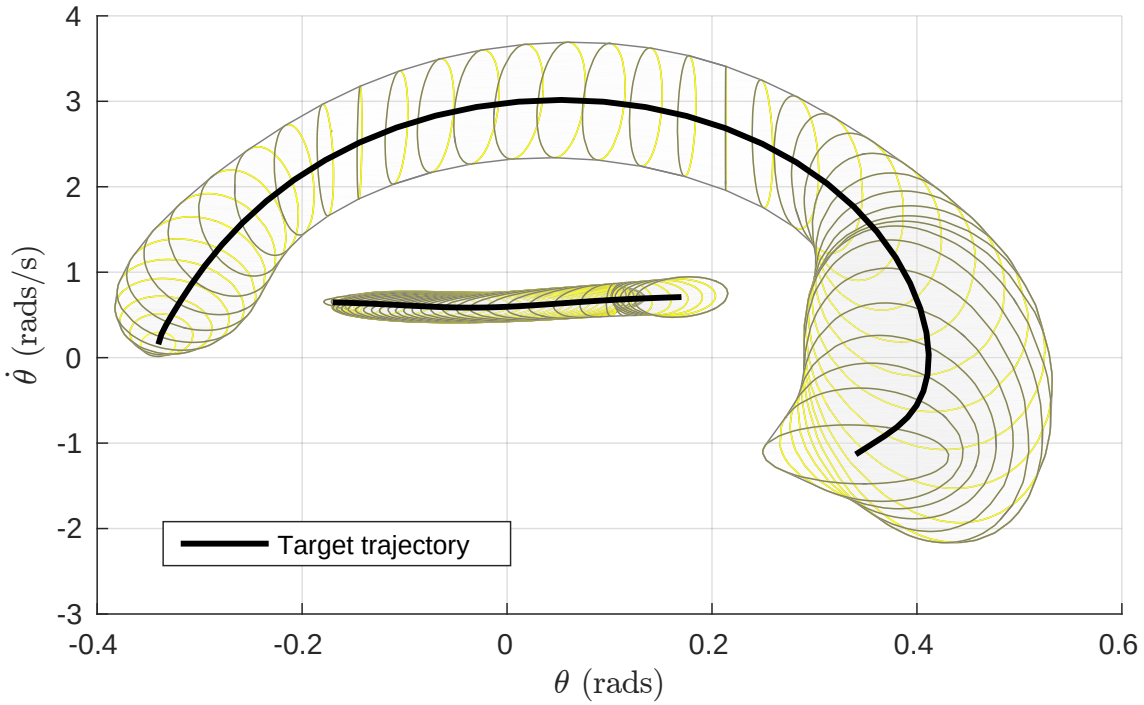

Figure 4.6 – Invariant funnel of the Compass Gait Walker.

Therefore, the strict forward invariance of the contracting region must be verified by ascertaining $V(x_\perp, \tau) = \rho \;\Rightarrow\; \dot{V}(x_\perp, \tau) < 0$.

4.6 Numerical results

4.6.1 Invariant Funnel and Stability Funnel of The Compass Gait Walker

Using the SPOTless toolbox [2] and commercial solver MOSEK version 7.1.0.46, we applied Algorithm 1 to compute an invariant funnel for our compass gait hardware model. The funnel is shown in Fig. 4.6.

We then applied Algorithm 2 to compute the contracting stability funnel for the same model, as shown in Figure 4.7. As is expected, the invariant funnel is larger in volume than that of the stability funnel because the former is a more relaxed condition.

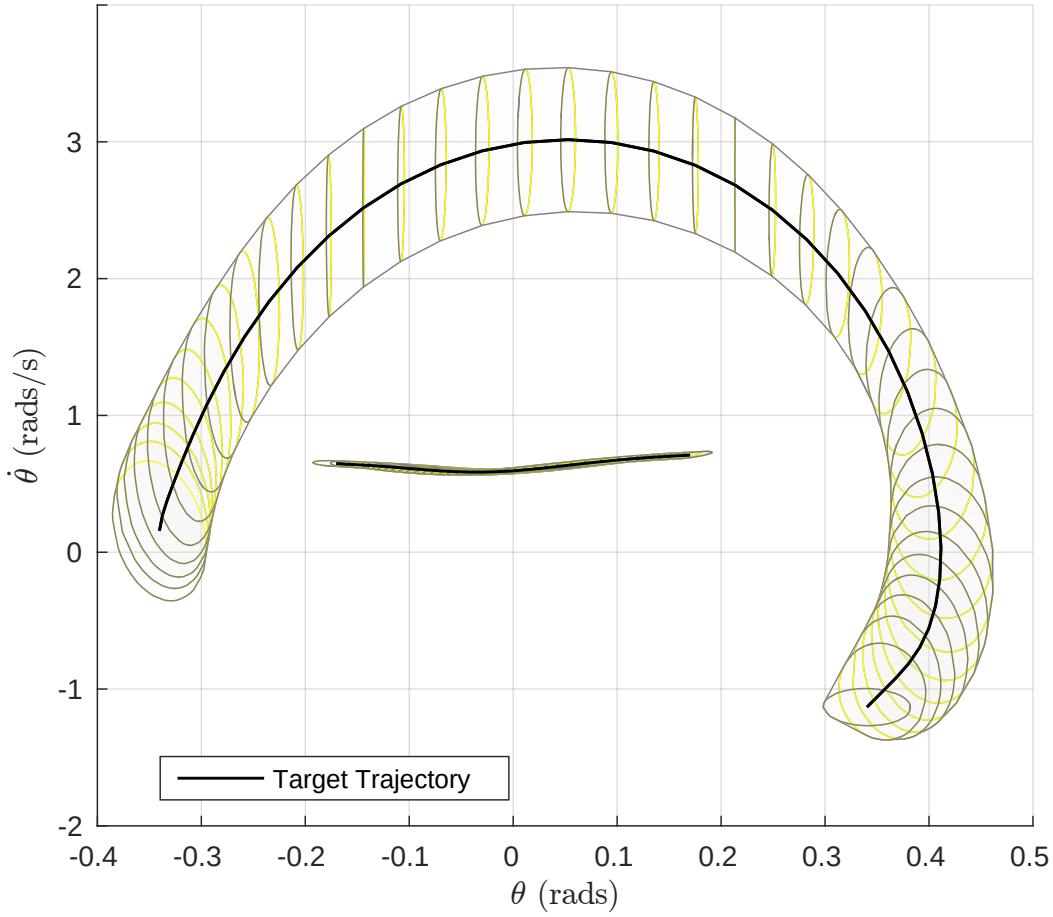

Figure 4.7 – Contraction region of the Compass Gait Walker.

Table 4.1 – Range of friction coefficients F_v for which the system is contracting w.r.t. the nominal metric

Verified region (as % of maximised ρ)	Bounds for F_v (multiples of the nominal value)	
	Lower Bound	Upper Bound
100%	0.0	12.2
80%	0.0	15.5
60%	0.0	18.5
40%	0.0	21.3
20%	0.0	24.0

4.6.2 Robustness of The Compass Gait Walker

We now show robustness analysis to parametric uncertainty for the compass gait walker by studying variations in the friction coefficient F_v.

First, using the metric from the nominal system, the upper and lower bounds for variations in F_v was found by respectively maximising and minimizing the error terms in the contraction conditions in (4.48) as discussed in Algorithm 3. The results are shown in Table 4.1.

As can be seen, the more conservative the region, the larger the bounds for uncertainty.

Second, we used Algorithm 3 to search for a new metric which maximises the upper bounds for F_v. Similar to methods used to enlarge the region, a bilinear search was used. The upper bound converges to 2.13e−2, or 17.1 times the original value, with 80% of ρ after five iterations. This represents a 9.7% increase in allowable friction coefficient over that for the nominal metric.

As noted in Section 3.5, the invariance condition needs to be separately checked when uncertainty is incorporated. This was ascertained by sampling the invariance condition, i.e. $V = \rho \Rightarrow \dot{V} < 0$, at 40,000 points along the surface of the funnel.

We now address several observations from our numerical implementation.

4.6.3 Accuracy of Taylor Series Expansion

As mentioned in Section 4.4-C, we used a third-order Taylor approximation along the limit cycle to verify the invariance conditions using SOS. Hence, it was vital to ensure the conditions are also satisfied on the original Euler-Lagrange model.

For verification, we sampled 40,000 states on the boundary of the funnel with the Euler Lagrange model; and all achieved the required $\dot{\dot{V}} < \dot{\rho}$.

4.6.4 Numerical performance and implementation details

The method outlined in this paper often results in large SOS programs which require special attention to numerical conditioning of the problem. Several strategies which the authors have successfully utilised to overcome numerical issues associated with large SOS problems are now discussed.

- **Numerical balancing**. Similar to [80], solutions to the jump-transverse-Riccati differential equation can have a large range of eigenvalues, particularly for underactuated systems such as the compass gait. In order to avoid numerical issues in semidefinite programming, it is vital to find a coordinate transformation

$$x_b = \mathbf{T}x$$

  where $\mathbf{T}$ numerically conditions the problem by ensuring the matrices $\mathbf{T}^T M_\perp \mathbf{T}$ from (4.38) and $\mathbf{T}^T(\mathbf{H}(J)))\mathbf{T}$ are as close to the identity matrix as possible; with $\mathbf{H}(J)$ being the Hessian of J from (4.37) evaluated at $x_\perp = 0$.

- **Solving a feasiblility problem to recover the analytic centre solution**. It is known that in practice, SDP solvers may not return strictly valid certificates for SOS programs, due to termination criteria and infeasible methods in these solvers, and fundamental limitations of floating-point implementations

[48]. This poses a problem in the ρ-step (line 6 of Algorithm 1) of our method as the SDP solver often returns a 'maximised' ρ that is slightly infeasible. The slightly questionable ρ in turn causes questionable solutions in the multiplier-step, thereby degenerating into worsening numerical problems in subsequent iterations. Solving the ρ-step problem twice – once as a *maximization* problem to optimize funnel volume; and a second time as a *feasibility* problem with a lower bound for the previously optimized objective – ensures a strictly feasible ρ is obtained at every iteration. This is shown Algorithm 4.

- **Using partial facial reduction.** We applied [65] and found simplifications could be found to reduce the dimensionality of resulting program by nearly 50%. For the problem formulations in both Algorithm 1 and 3, simplifications were consistently found in the *multiplier-step*, while no simplifications were found in the $\rho-step$ or $\epsilon-step$.

Algorithm 4 Backtracking Algorithm for Obtaining Strictly Feasible Funnel for the ρ-step in Line 6 of Algorithm 1

```
1: strictlyFeasible = 0;
2: backtrackingMargin = 0.9;
3: Maximisation-step: Fix l_1, l_2 and maximise the
       objective ρ in (4.24) satisfying (4.25) to (4.29).
4: feasibleCandidate = ρ;
5: while not strictlyFeasible do
6:     ρ =feasibleCandidate;
7:     Feasibility-step: Fix l_1, l_2, ρ, and solve feasibility
        problem satisfying (4.25) to (4.29).
8:     if Feasibility-step succeeds then
9:         strictlyFeasible = 1;
10:    else
11:        feasibleCandidate = ρ×backtrackingMargin;
12:    end if
13: end while
```

4.6.5 Example Implementation

A MATLAB implementation of the framework outlined herein has been made available online at [1].

4.7 Conclusion

We have developed a simplified analytical framework which systematically generates an inner-estimate of the region of stability for walking motions under virtual constraints. This framework enables rigorous comparison of global stability properties for different virtual constraint candidates and controllers, vital for informed design decisions.

While the compass gait walker has been used as illustration in this paper, this framework is applicable to higher dimensional systems and will be the focus of future work.

Chapter 5

Hardware Experimental Verifications

5.1 Introduction

In this chapter we present a hardware compass gait walker platform as introduced in Chapter 4, with aims of demonstrating the utility of the new proposed transverse coordinates and computation of stability funnels in a physical setup.

The work presented in this chapter has been partially published in [9] and [79]. In [9], this author was responsible for the system identification portion of the paper which is the focus of the first half of this chapter.

5.2 Hardware bipedal walker setup

Given the compass-gait model is a planar walking model, a common way of realizing it in our three-dimensional reality is to mount the walker to a rotating boom (e.g., [19]). In our setup, the rotating boom is made of carbon fibre tube for its light weight and high stiffness. The boom is supported by a pole forming the centre of the walking circle, constraining the robot to walk along a circle of 2.2m radius, which is a sufficient approximation of a planar walking motion as there is only 42mm distance between both toes when the legs are parallel. A counterweight of 5kg set at a distance of $78cm$

from the central pole is used to make the net weight of the walker lighter to avoid damaging some components and ensure that the servos could support the walker during impacts. Figure 5.1 shows the hardware walker along with the schematic diagram of the compass gait walker.

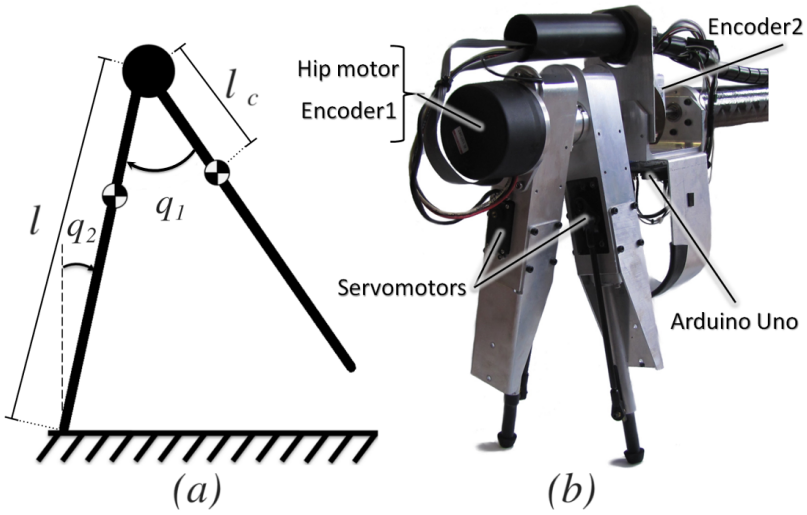

Figure 5.1 – The Compass Gait Walker Hardware

The motor is directly connected to both legs, avoiding backlash and additional friction and inertia that would be introduced by a gearbox system. The stator is mounted on the outer leg and the rotor is connected to the inner leg.

The walker is equipped with two incremental encoders. Encoder 1 (Figure 5.1(b)) measures the angle between both legs ψ_1, whereas Encoder 2 measures the angle of the inner leg with respect to the boom ψ_2. Hence, swing leg angle q_1 and the stance angle q_2 are derived as follows:

- when inner leg is stance $\rightarrow q_1 = \psi_1$ and $q_2 = -\psi_2$.
- when outer leg is stance $\rightarrow q_1 = -\psi_1$ and $q_2 = -\psi_2 + \psi_1$.

Table 5.1 – Fixed vs free parameters in Experiment 1 and Experiment 2

Variable	**Expt 1**	**Expt 2**
Leg mass m [kg]	fixed	fixed
Leg length l [m]	fixed	fixed
Gravitational hip mass m_{Hg} [kg]	—	fixed
Inertia I_c [kgm^2]	free	fixed
Length to COM l_c [m]	free	fixed
Coulomb friction Fc [Nm]	free	fixed
Viscous friction Fv [Nms]	free	fixed
Inertial hip mass m_H [kg]	—	free

5.3 Parameter Estimation

Because of the large number of model parameters which needed to be identified, we have performed the parameter estimation process over two seperate experiments, enabling different parameters to be identified independently as much as possible. This approach avoids over-fitting and improves the identifiability of the system.

Firstly, the mass m and length l of each leg were easily measured using a scale and a ruler, respectively. Similarly, the gravitational hip mass m_{Hg} (i.e. the net weight of the walker mounted on the boom minus the weight of the legs) is also easily measurable using a scale. Now that these parameters have been established, we consider them to be fixed in the remaining experiments.

We now describe the two experiments used to identify the remaining parameters. Table 5.1 shows the 'free' and 'fixed' parameters for each experiment – the free parameters are the ones being estimated in each respective experiment.

5.3.1 Experiment 1: Simple Pendulum Model

In the first case, the walker is set up such that its motion replicate a simple pendulum with dynamics as follows.

$$I_c\ddot{q}_1 = \Gamma - mgl_c\sin(q_1) - F(\dot{q}_1), \tag{5.1}$$

where the torque $\Gamma = K_t u$; I_c the inertia of a single leg; and $F(\dot{q}_1) = F_v\dot{q}_1 + F_c sign(\dot{q}_1)$ the friction (F_v and F_c are respectively viscous and coulomb friction). The data collection for this experiment is summarised as follows.

Experiment 1

Aim: Identify I_c, l_c, F_v, F_c for each leg.

Objective function:

$$\min_{I_c, l_c, F_v, F_c} \int_{t_0}^{t_f} \|y(t) - \hat{y}(t)\|^2 dt$$

where $y(t)$ are the recorded angles, and $\hat{y}(t)$ are the simulated angles $q(t)$ using (5.1).

Fixed parameters: m, g, K_t

Procedure:

1. Fix the inner leg at its downward equilibrium.
2. Start logging data.
3. Lift the other leg to the horizontal (so as to make the hip angle 90°), then release to achieve a free-swinging motion. Let the leg settle at its downward equilibrium.
4. Actuate the motor with a square pulse with 90mNm magnitude and a period of 10 seconds. Do this for three cycles, and let the leg settle again.
5. Actuate the motor with a 55mNm chirp ranging from 0.5 to 60Hz over a 60 second interval.
6. Stop logging data.
7. Repeat steps 1-6 with the outer leg fixed, and record the inner leg swinging.
8. Perform minimization of the above objective function for each leg separately.

This simple pendulum model leads to an estimate of F_c and F_v, and gives values for the leg's inertia I_c as well as the length to center of mass (COM) l_c. These values will in turn be used in the full compass-gait model of the walker, thus reducing the number of parameters left to be estimated.

We used MATLAB's built-in parameter estimation toolbox to perform a nonlinear least squares fit using the trust-region-reflective algorithm.

Figure 5.2 represents the friction $f(\dot{q}_1)$ as a function of the angular velocity of the swing leg, which is obtained by differentiating the filtered angular position using a zero phase Butterworth lowpass filter (12th order, half power frequency of 0.15). As the figure suggests, that viscous and coulomb friction terms alone are insufficient to perfectly describe the complex effects of friction of the walker. However, given that the walker is mostly operating in low speed (less than 2 rad/s), it is deemed that such model is sufficient. Table 5.2 shows the results of parameter estimation on Experiment 1. Figure 5.4 and Figure 5.3 show the free swing motion for the inner and outer leg, respectively.

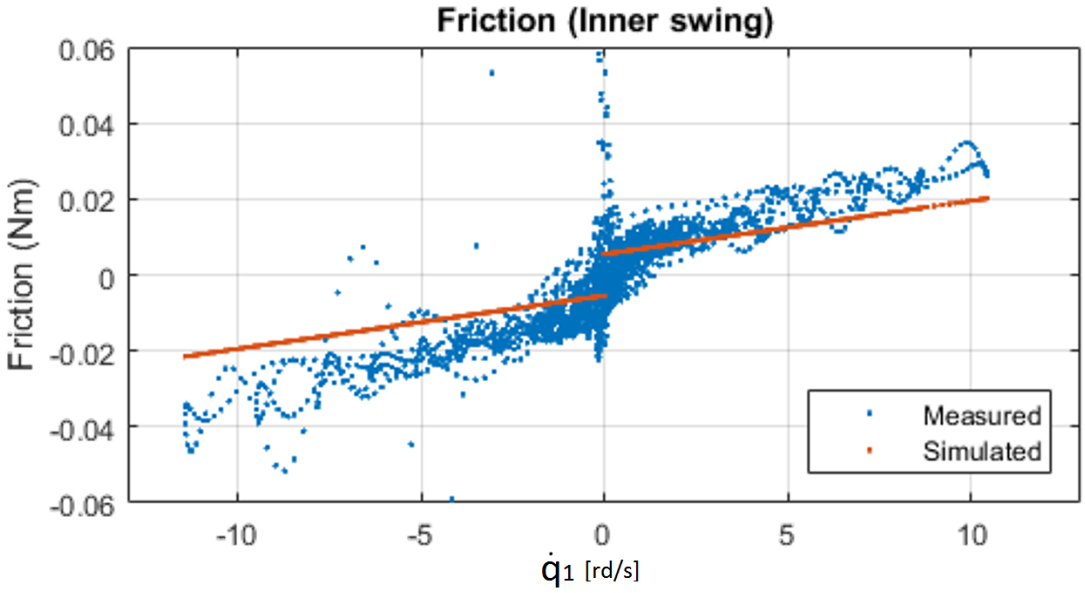

Figure 5.2 – Friction identification using Experiment 1

There is a minor difference in the behaviour of the inner leg compared to the outer

Table 5.2 – Measured and identified parameters from Experiment 1

Variable	Initial guess	Inner leg	Outer leg
K_t [mNm/V]	–	18.3	18.3
m [kg]	–	0.7	0.7
m_{Hg} [kg]	–	−0.4	−0.4
l [m]	–	0.278	0.278
Fc [Nm]	$2e^{-3}$	$5.4434e^{-3}$	$6.7777e^{-3}$
Fv [Nms]	$2e^{-3}$	$1.4038e^{-3}$	$1.7189e^{-3}$
l_c [m]	$4.37e^{-2}$	$4.4754e^{-2}$	$5.0154e^{-2}$
I_c [kgm^2]	$3e^{-3}$	$4.3238e^{-3}$	$4.3694e^{-3}$

leg, possibly due to the cables connecting the motor to the rest of the hardware.

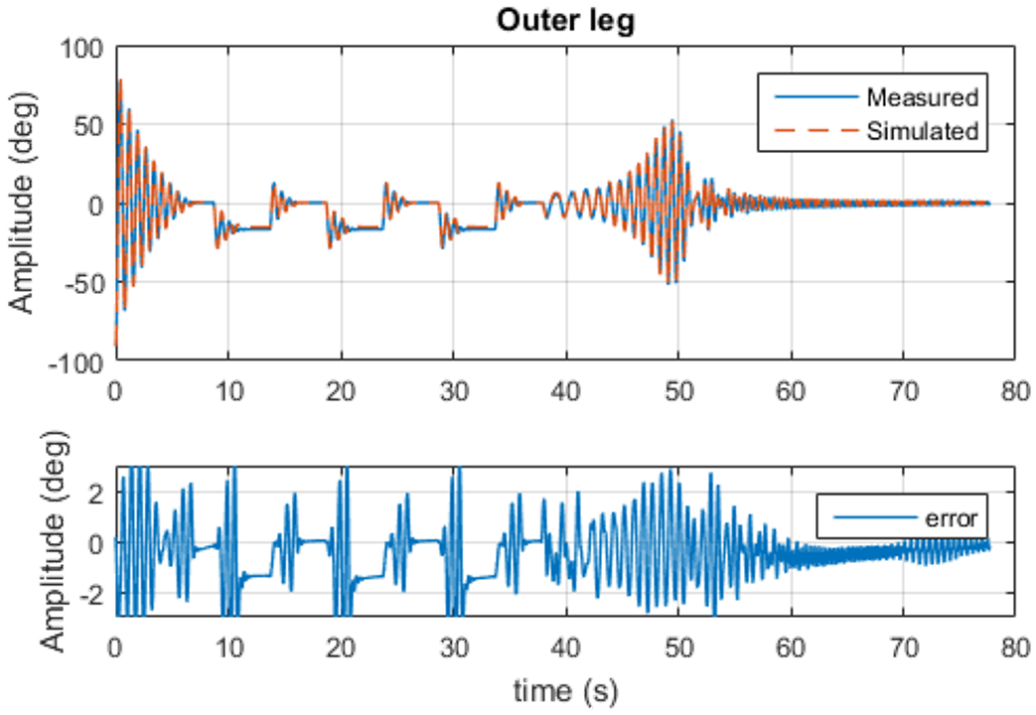

Figure 5.3 – Outer leg model and hardware response comparison.

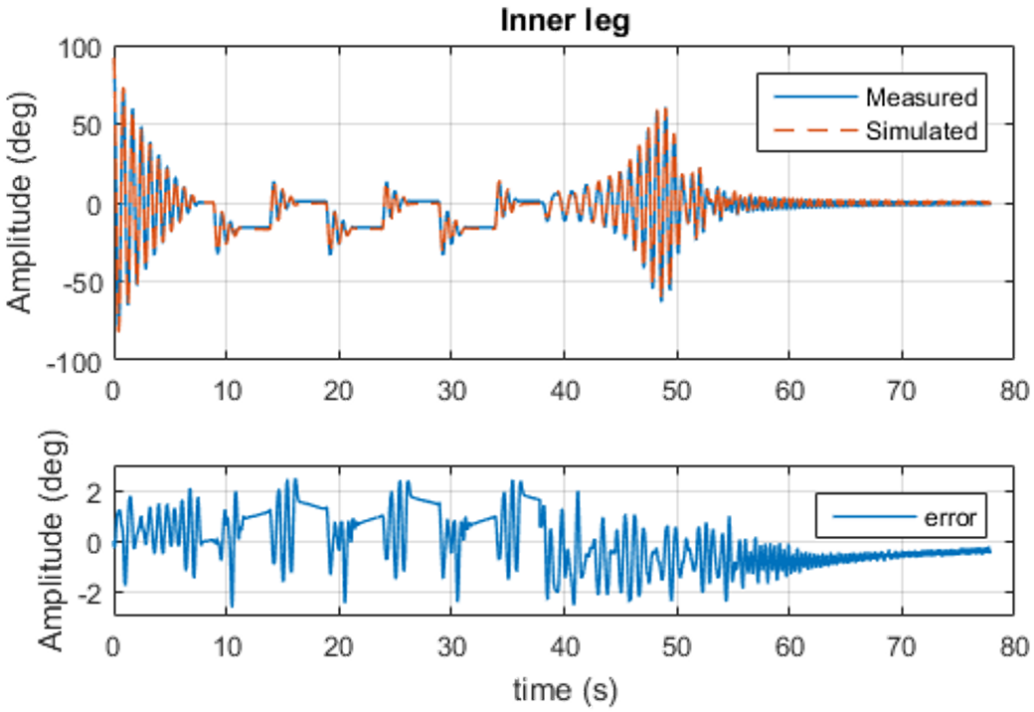

Figure 5.4 – Inner leg model and hardware response comparison.

5.3.2 Experiment 2: Compass-Gait Model with Friction

Using the parameters identified from Experiment 1, the only remaining unidentified parameter of the walker – the hip mass, m_H – can now be identified by fitting walking data to a modified compass gait dynamical model.

Dynamical model of the compass gait walker

Due to the mechanical construction specific to this walker, the traditional compass gait walker model has been modified to reflect the physical properties of the hardware setup.

Firstly, adjustments were made to cater for the fact that the robot is mounted on a boom arm with a counterweight, and therefore walks in a circular path. The dynamical effect of the boom and the counterweight is approximated by using a different hip mass for inertial (m_H) and gravitational (m_{H_g}) terms in the model.

Secondly, the masses, COM, and inertia of either legs in the walker are not exactly identical due to cables and motor attachments. This causes the robot to be slightly asymmetric – in contrast with the classical compass gait walker model which assumes symmetry between the two legs. This issue is addressed by including separate masses, COMs and inertias for the swing and stance legs in the model.

The dynamical model of the compass gait walker with viscous friction (F_v) and Coulomb friction (F_c) terms are shown in compressed form in (5.2). The full model can be found in Appendix A.

$$M(q)\ddot{q} + C(q,\dot{q})\dot{q} + G(q) = B(q)(u - F(\dot{q})) \tag{5.2}$$

Experimental Design

It is well known that parameter estimation for closed loop systems is inherently difficult due to issues with identifiability, see e.g.,[83]. To overcome the identifiability issues and avoid over-fitting to a particular walking gait, the walking data was collected using three different control strategies, with and without a feedback control, as well as a parallel combination of the two.

The procedure of Experiment 2 is summarised below.

Experiment 2

Aim: Identify the m_H for each leg.

Objective function:

$$\min_{m_H} \sum_i \int_0^T \|y(t) - \hat{y}(t)\| dt. \tag{5.3}$$

where y represents the measured angles and $\hat{y}$ represents the angles from simulated dynamics

Procedure:

1. Select four virtual constraints (VCs) as reference trajectories.

Table 5.3 – Identified Parameter from Experiment 2

Robot Side	**Identified m_H value (kg)**	Variance
Inner-leg as Stance leg	1.00	1.62×10^{-3}
Outer-leg as Stance leg	1.00	1.49×10^{-3}

2. Select three controllers – one feedback controller, one feedforward controller and one parallel combination of the two as follows:
   - PD controller
   - Phase indexed Iterative Learning Controller (ILC)
   - PD controller and phase indexed ILC as described in [44]
3. For each combination of reference trajectory and controller, record walking motion for the walker until stable walking motion is achieved for at least 50 steps.
4. From each run, select 9 to 10 consecutive steps of stable walking motion to form the data to be used in the parameter estimation.

The data collected in Experiment 2 is first processed to segment the continuous phase of every step. For better identification of the continuous dynamics, vibration associated with foot impact are eliminated from the data by removing 20 milliseconds of data immediately before and after impact.

The segmented and processed data are then used in the estimation of the hip mass (m_H) using MATLAB's nonlinear grey-box estimation toolbox, with nonlinear least-squares to minimize output error. The identified value from both sides of the walker are shown in Table 5.3. As the results demonstrate, both sides of the asymmetric model result in an identical hip mass as per physical intuition.

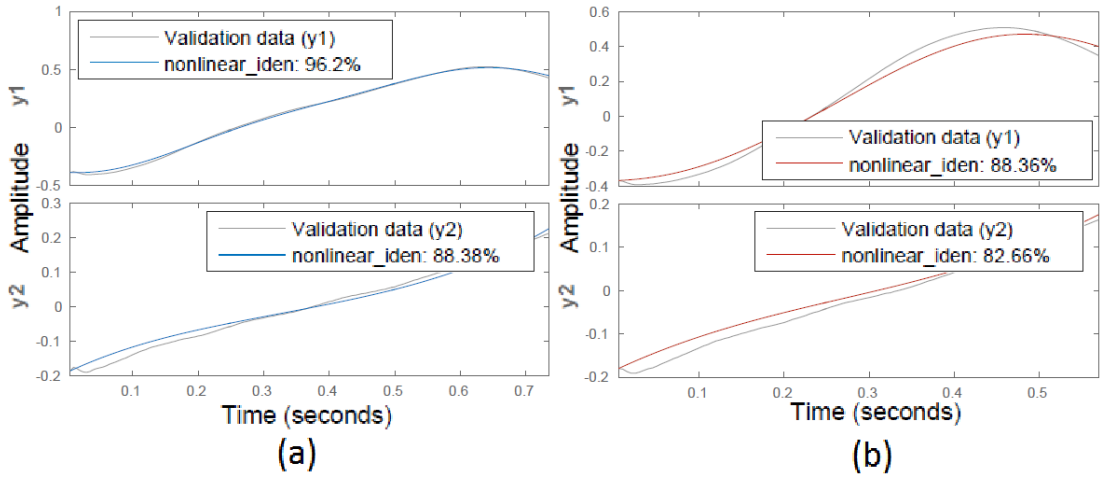

Figure 5.5 – Real data and identified model of the continuous dynamics. Best (a) and worst (b) fitting from 114 steps of Experiment 2.

5.4 Experimental Results for Funnel Verification

We used the compass gait walker to test – in hardware – the efficacy of the proposed transverse coordinate construction, the transverse-LQR controller, and the verified invariant funnels computed in Section 4.6.

Figure 5.6 shows the phase portrait of 15 steps for the walker while in stable walking motion. Note that while the vibrations from the boom could be observed in the stance leg; the trajectory remained within the invariant funnel as predicted. The only exception occurs at the very beginning of a few steps, which can be attributed to the vibrations during impact, unaccounted for in our impact model which assumes an inelastic collision with no slip or bounce.

To test the behaviour of the system closer to the boundary of the invariant funnel, a disturbance torque in the hip motor was applied at various stages of a step. The results are shown in Figure 5.7. Note that all trajectories successfully re-enter or remain in the invariant funnel after the disturbance torque has been applied.

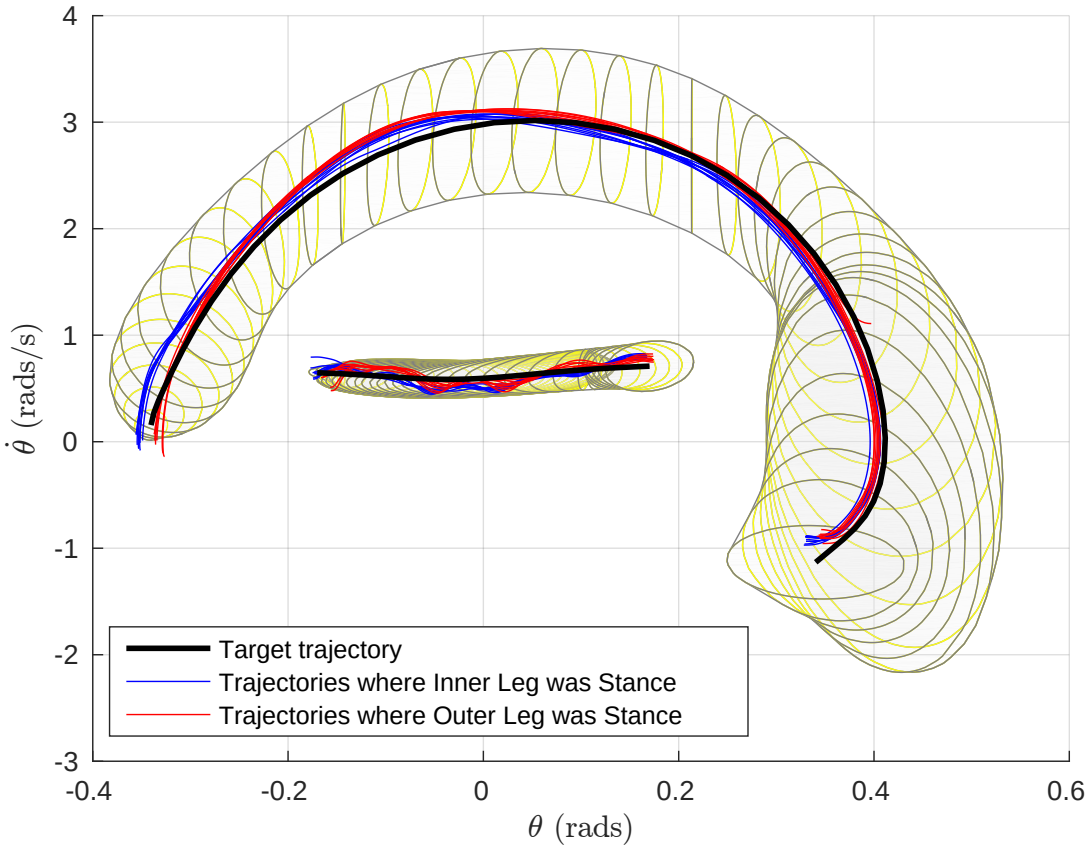

Figure 5.6 – Hardware experimental results superimposed with the computed invariant funnel.

5.5 Summary

In this chapter we outlined the design and construction of a hardware compass gait walker. Extensive experiments were done for accurate parameter estimation . The resulting model was used to construct transversal coordinates and forward invariant funnels as per Chapter 4. The funnels were then successfully verified in hardware.

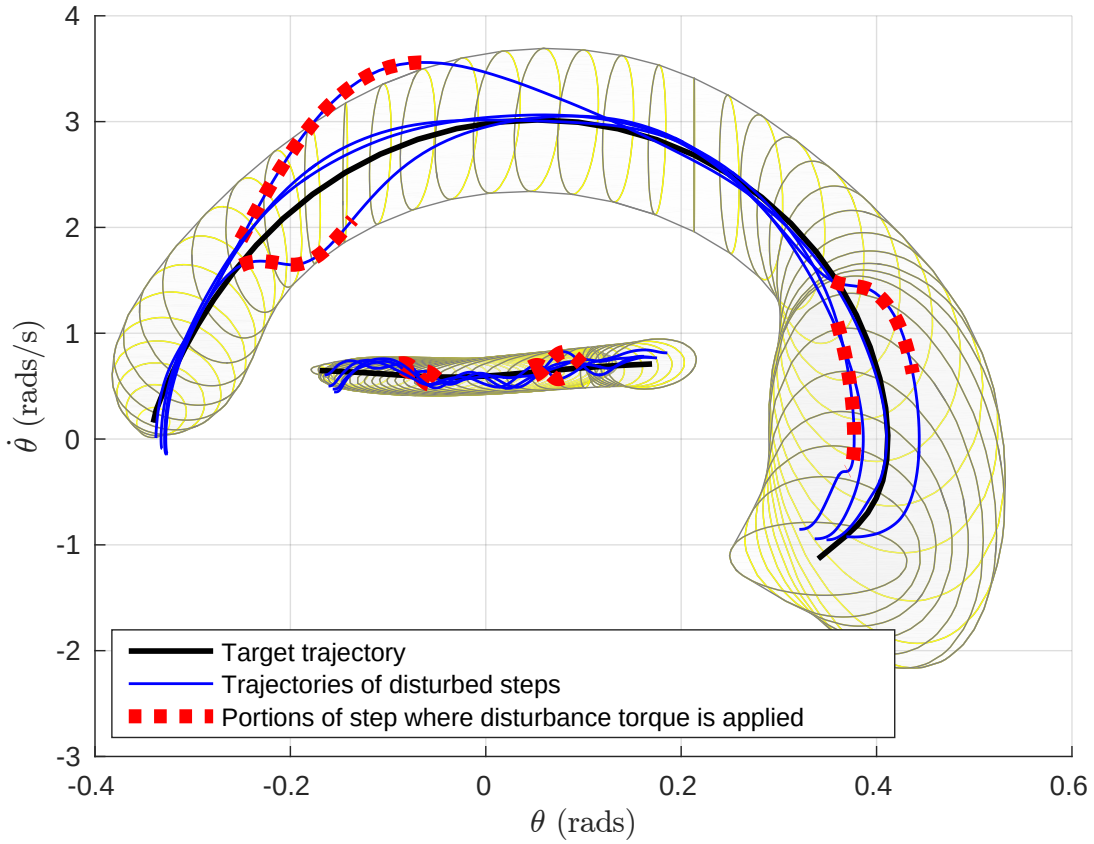

Figure 5.7 – Experimental results where disturbance torques were applied to the hip motor. Note that all trajectories either (a) successfully re-enters the invariant funnels after the disturbance; or (b) remain in the invariant funnel throughout the disturbance.

Chapter 6

Conclusion

This thesis has proposed new theoretical methods to analyse stability and robustness of periodic walking motions. The computational implementation of the methods using convex optimisation tools were also extensively discussed to demonstrate numerical tractability. Finally, physical hardware verification on a bipedal walker was successfully implemented.

6.1 Summary

In **Chapter 2**, current work in the field of stability analysis for nonlinear and hybrid systems was discussed, highlighting the difficulties in analysing the stability of dynamic walking robot motion.

In **Chapter 3**, the new transverse contraction analysis framework for hybrid nonlinear limit cycles was introduced, enabling stability and robustness analysis of such systems. Unlike traditional Lyapunov-based tools, the contraction framework developed in this thesis enables proof of stability without prior knowledge of the exact location of the limit cycle in state space. Numerical application example on a dynamic walking robot – the rimless wheel – was also successfully implemented.

Chapter 4 demonstrates that for nonlinear systems with higher dimensions, a simplified construction of the transverse coordinates is possible for typical models of underactuated walking robots. This enables more efficient computation of stability certificate in the reduced coordinates.

To validate the work in Chapter 3 and Chapter 4, a physical walking robot – the Compass Gait walker – was implemented in **Chapter 5**. System identification of the walker was carried out and stability analysis via the methods proposed in this thesis was implemented. Hardware experiments successfully verified the computational results.

6.2 Future Work

This thesis has demonstrated the computation of stability funnels for dynamic walking robots via convex optimisation tools. This is an enabling technology for numerous practical problems which should be the focus of future works.

While the rimless wheel and the compass gait walker has been used as illustration in this thesis, the framework proposed herein is applicable to higher dimensional systems and would naturally be the focus on future work. Such studies would include more sophisticated walking models, for example the 3-link or 5-link walker as illustrated in [85]. It is commonly known that SOS scales poorly with dimensionality and therefore works such as DSOS and SDSOS by [4, 53] would be vital for numerical tractability of the resulting problem.

Further, the stability analysis tools developed in this thesis can be applied to evaluate competing robot designs. It can also be used to construct switching feedback controllers with guaranteed stability. These applications would enable a more systematic and informed design approach for robots based on their stability and robustness properties.

Bibliography

[1] Simplified Construction for Stability Funnels for the Compass Gait Walker: Example MATLAB Code. Available Online: http://www-personal.acfr.usyd.edu.au/ian/doku.php?id=wiki:software.

[2] SPOTless: Systems Polynomial Optimization Toolbox.

[3] Rimless Wheel transverse contraction example. Available Online: http://www-personal.acfr.usyd.edu.au/ian/doku.php?id=wiki:software. 2014.

[4] A. A. Ahmadi and P. A. Parrilo. Towards Scalable Algorithms with Formal Guarantees for Lyapunov Analysis of Control Systems via Algebraic Optimization. Technical report.

[5] P. Antsaklis, J. Stiver, and M. Lemmon. Hybrid system modeling and autonomous control systems. *Hybrid Systems, Lectures Notes in Computer Science*, 736:366–392, 1993.

[6] E. M. Aylward, P. A. Parrilo, and J.-J. E. Slotine. Stability and robustness analysis of nonlinear systems via contraction metrics and SOS programming. *Automatica*, 44(8):2163–2170, Aug 2008.

[7] P. A. Bhounsule, J. Cortell, A. Grewal, B. Hendriksen, J. G. D. Karssen, C. Paul, and A. Ruina. Low-bandwidth reflex-based control for lower power walking: 65 km on a single battery charge. *The International Journal of Robotics Research*, 33(10):1305–1321, 2014.

[8] S. Bittanti and P. Colaneri. *Periodic systems: filtering and control.* Springer-Verlag, London, 2008.

[9] A. M. Boudali, F. H. Kong, J. Martinez, J. Z. Tang, and I. R. Manchester. Design and Modeling of an Open Platform for Dynamic Walking Research. In *Proceedings of the IEEE International Conference on Mechatronics*, 2017.

[10] S. Boyd and L. Vandenberghe. *Convex Optimization.* Cambridge University Press, 2010.

[11] S. Boyd, L. E. Ghaoui, E. Feron, and V. Balakrishnan. *Linear matrix inequalities in system and control theory (Studies in applied mathematics, 15)*. 1994.

[12] M. S. Branicky. Stability of Hybrid Systems : State of the Art. (December): 120–125, 1997.

[13] M. S. Branicky. Stability of hybrid systems. In *Handbook of Networked and Embedded Control Systems*, pages 91–116. 2005.

[14] K. Byl and R. Tedrake. Metastable Walking Machines. *The International Journal of Robotics Research*, 28(8):1040–1064, Aug 2009.

[15] C. Byrnes. Topological Methods for Nonlinear Oscillations. *Notices of the AMS*, 57(9):1080–1091, 2010.

[16] J. Candy. A Use of Limit Cycle Oscillations to Obtain Robust Analog-to-Digital Converters. *IEEE Transactions on Communications*, 22(3): 298–305, Mar 1974.

[17] A. Chakraborty, P. Seiler, and G. J. Balas. Susceptibility of F/A-18 Flight Controllers to the Falling-Leaf Mode: Nonlinear Analysis. *Journal of Guidance, Control, and Dynamics*, 34(1):73–85, Jan 2011.

[18] G. Chen. Stability of Nonlinear Systems. *Encyclopedia of RF and Microwave Engineering*, (December):4881–4896, 2004.

[19] C. Chevallereau, G. Abba, Y. Aoustin, F. Plestan, E. Westervelt, C. Canudas-de Wit, and J. Grizzle. RABBIT: A testbed for advanced control theory. *IEEE Control Systems Magazine*, 23(5):57–79, Oct 2003.

[20] M. J. Coleman. *A Stability Study of a Three-Dimensional Passive-Dynamic Model of a Human Gait*. PhD thesis, Cornell University, 1998.

[21] S. Collins, A. Ruina, R. Tedrake, and M. Wisse. Efficient bipedal robots based on passive-dynamic walkers. *Science*, 27(5712):789, Oct 2005.

[22] H. Dai and R. Tedrake. L2-gain optimization for robust bipedal walking on unknown terrain. In *2013 IEEE International Conference on Robotics and Automation*, pages 3116–3123. IEEE, May 2013.

[23] R. Decarlo, M. Branicky, S. Pettersson, and B. Lennartson. Perspectives and results on the stability and stabilizability of hybrid systems. *Proceedings of the IEEE*, 88(7):1069–1082, Jul 2000.

[24] M. di Bernardo and D. Fiore. Incremental Stability of bimodal Filippov Systems in Rn. In *53rd IEEE Conference on Decision and Control*, pages 4679–4684. IEEE, Dec 2014.

[25] M. di Bernardo and D. Liuzza. Incremental Stability of Planar Filippov Systems. In *European Control Conference*, pages 3706–3711, 2013.

[26] K. El Rifai and J. J. E. Slotine. Compositional contraction analysis of resetting hybrid systems. *IEEE Trans. Automat. Contr.*, 51(9):1536–1541, 2006.

[27] R. Field and R. Noyes. Oscillations in chemical systems. IV. Limit cycle behavior in a model of a real chemical reaction. *Journal of Chemical Physics*, 60(March):1877–1884, 1974.

[28] D. Fiore, S. J. Hogan, and M. di Bernardo. Contraction analysis of switched Filippov systems via regularization. *Automatica*, 73:279–288, 2016.

[29] L. Freidovich, A. Shiriaev, and I. Manchester. Stability analysis and control design for an underactuated walking robot via computation of a transverse linearization. *Proc. 17th IFAC World Congress*, pages 10166–10171, 2008.

[30] J. M. Gonçalves. Regions of stability for limit cycle oscillations in piecewise linear systems. *Automatic Control, IEEE Transactions on*, 50(11):1877–1882, 2005.

[31] J. M. Gonçalves, A. Megretski, and M. A. Dahleh. Global analysis of piecewise linear systems using impact maps and surface Lyapunov functions. *Automatic Control, IEEE Transactions on*, 48(12):2089–2106, 2003.

[32] R. D. Gregg, A. K. Tilton, S. Candido, T. Bretl, and M. W. Spong. Control and Planning of 3-D Dynamic Walking With Asymptotically Stable Gait Primitives. *IEEE Transactions on Robotics*, 28(6):1415–1423, Dec 2012.

[33] J. W. Grizzle, C. Chevallereau, R. W. Sinnet, and A. D. Ames. Models, feedback control, and open problems of 3D bipedal robotic walking. *Automatica*, 50(8):1955–1988, 2014.

[34] J. Guckenheimer and P. Holmes. *Nonlinear Oscillations, Dynamical Systems, and Bifurcations of Vector Fields*. Springer-Verlag, 1997.

[35] W. M. Haddad and V. S. Chellaboina. *Nonlinear dynamical systems and control: a Lyapunov-based approach*. Princeton University Press, New Jersey, 2008.

[36] J. K. Hale. *Ordinary Differential Equations*. Robert E. Krieger Publishing Company, New York, Jan 1980.

[37] J. Hauser and C. C. Chung. Converse Lyapunov functions for exponentially stable periodic orbits. *Systems & Control Letters*, 23(1):27–34, Jul 1994.

[38] I. Hiskens. Stability of hybrid system limit cycles: application to the compass gait biped robot. *Proceedings of the 40th IEEE Conference on Decision and Control (Cat. No.01CH37228)*, 1:774–779, 2001.

[39] D. Hobbelen and M. Wisse. A Disturbance Rejection Measure for Limit Cycle Walkers: The Gait Sensitivity Norm. *IEEE Transactions on Robotics*, 23(6): 1213–1224, Dec 2007.

[40] C. S. Hsu. A Theory of Cell-to-Cell Mapping Dynamical Systems. *Journal of Applied Mechanics*, 47(4):931–939, 1980.

[41] M. Johansson and A. Rantzer. Computation of piecewise quadratic Lyapunov functions for hybrid systems. *IEEE Transactions on Automatic Control*, 43(4): 555–559, Apr 1998.

[42] J. Jouffroy and T. I. Fossen. Tutorial on Incremental Stability Analysis using Contraction Theory. *Modeling, Identification and Control: A Norwegian Research Bulletin*, 31(3):93–106, 2010.

[43] H. K. Khalil. *Nonlinear systems*. Prentice Hall, Upper Saddle River, 3rd edition, 2002.

[44] F. H. Kong, A. M. Boudali, and I. R. Manchester. Phase-indexed ILC for control of underactuated walking robots. In *2015 IEEE Conference on Control and Applications, CCA 2015 - Proceedings*, pages 1467–1472, 2015.

[45] G. A. Leonov. Generalization of the Andronov-Vitt Theorem. *Regular and Chaotic Dynamics*, 11(2):281–289, 2006.

[46] G. A. Leonov. Shukovsky Stability in Dynamical Systems. Generalization of Andronov-Witt Theorem. *The 3rd International IEEE Scientific Conference on Physics and Control*, pages 78–80, 2007.

[47] J. Lofberg. YALMIP: A toolbox for modeling and optimization in MATLAB. *IEEE International Symposium on Computer Aided Control Systems Design*, 2004.

[48] J. Lofberg. Pre-and post-processing sum-of-squares programs in practice. *Automatic Control, IEEE Transactions on*, 54(5):1007–1011, 2009.

[49] W. Lohmiller. *Contraction analysis of nonlinear systems*. PhD thesis, MIT, 1999.

[50] W. Lohmiller and J.-J. E. Slotine. On Contraction Analysis for Non-linear Systems. *Automatica*, 34(6):683–696, Jun 1998.

[51] W. Lohmiller and J.-J. E. Slotine. Nonlinear process control using contraction theory. *AIChE Journal*, 46(3):588–596, Mar 2000.

[52] A. Majumdar, A. A. Ahmadi, and R. Tedrake. Control design along trajectories with sums of squares programming. In *Proceedings - IEEE International Conference on Robotics and Automation*, pages 4054–4061, Oct 2013.

[53] A. Majumdar, A. A. Ahmadi, and R. Tedrake. Control and Verification of High-Dimensional Systems with DSOS and SDSOS Programming. *Proceedings of the 53rd the IEEE Conference on Decision and Control*, 2014.

[54] I. R. Manchester. Transverse dynamics and regions of stability for nonlinear hybrid limit cycles. *Proceedings of the IFAC World Congress 2011 (extended version at arXiv:1010.2241)*, pages 1–9, Oct 2011.

[55] I. R. Manchester and U. Mettin. Stable dynamic walking over uneven terrain. *The International Journal of Robotics Research*, 30(3):265–279, Jan 2011.

[56] I. R. Manchester and J.-J. E. Slotine. Transverse contraction criteria for existence, stability, and robustness of a limit cycle. *Systems & Control Letters*, 63:32–38, Sep 2014.

[57] I. R. Manchester, M. M. Tobenkin, M. Levashov, and R. Tedrake. Regions of Attraction for Hybrid Limit Cycles of Walking Robots. In *Proceedings of the IFAC World Congress 2011 (extended version at arXiv: 1010.2247)*, Oct 2011.

[58] T. McGeer. Dynamics and control of bipedal locomotion. *Journal of theoretical biology*, 163(3):277–314, 1993.

[59] D. Merkin. *Introduction to the Theory of Stability*. Springer-Verlag, New York, 1997.

[60] J. Moore, R. Cory, and R. Tedrake. Robust post-stall perching with a simple fixed-wing glider using LQR-Trees. *Bioinspiration & biomimetics*, 9(2):025013, 2014.

[61] L. Ning, L. Junfeng, and W. Tianshu. The effects of parameter variation on the gaits of passive walking models: simulations and experiments. *Robotica*, 27(04): 511, 2009.

[62] P. A. Parrilo. Structured semidefinite programs and semialgebraic geometry methods in robustness and optimization. 2000, 2000.

[63] P. A. Parrilo. Semidefinite programming relaxations for semialgebraic problems. *Mathematical Programming*, 96(2):293–320, May 2003.

[64] P. A. Parrilo and S. Lall. Semidefinite Programming Relaxations and Algebraic Optimization in Control. *European Journal of Control*, 9(2-3):307–321, Jun 2003.

[65] F. Permenter and P. Parrilo. Partial facial reduction: simplified, equivalent SDPs via approximations of the PSD cone. *arXiv*, pages 1–38, 2014.

[66] Q.-C. Pham. Analysis of discrete and hybrid stochastic systems by nonlinear contraction theory. In *2008 10th Int. Conf. Control. Autom. Robot. Vis.*, number December, pages 1054–1059. IEEE, dec 2008.

[67] Q. C. Pham and J. J. Slotine. Stable concurrent synchronization in dynamic system networks. *Neural Networks*, 20(1):62–77, 2007.

[68] H. Poincaré. Memoire sur les courbes definies par une equation differentielle. *Journal de mathematiques pures et appliquees*, 7(I):375–422, 1881.

[69] S. Prajna, A. Papachristodoulou, and P. A. Parrilo. Introducing SOSTOOLS: a general purpose sum of squares programming solver. *Proceedings of the 41st IEEE Conference on Decision and Control, 2002.*, 1(2):741–746, 2002.

[70] G. Russo and M. di Bernardo. Contraction Theory and Master Stability Function: Linking Two Approaches to Study Synchronization of Complex Networks. *IEEE Transactions on Circuits and Systems II: Express Briefs*, 56 (2):177–181, Feb 2009.

[71] A. L. Schwab and M. Wisse. Basin of attraction of the simplest walking model. *ASME Design Engineering Technical Conference*, 2001.

[72] J. A. Scott Kelso, K. G. Holt, P. Rubin, and P. N. Kugler. Patterns of Human Interlimb Coordination Emerge from the Properties of Non-Linear, Limit Cycle Oscillatory Processes. *Journal of Motor Behavior*, 13(4):226–261, Dec 1981.

[73] A. S. Shiriaev, L. B. Freidovich, and I. R. Manchester. Can we make a robot ballerina perform a pirouette? Orbital stabilization of periodic motions of underactuated mechanical systems. *Annual Reviews in Control*, 32(2):200–211, Dec 2008.

[74] J.-J. E. Slotine, W. Wang, and K. El-Rifai. Contraction analysis of synchronization in networks of nonlinearly coupled oscillators. *Proc. 16th Int. Symp. Mathematical Theory of Networks and Systems*, pages 1–18, 2004.

[75] J. F. Sturm. Using SeDuMi 1 . 02 , a MATLAB toolbox for optimization over symmetric cones 1 Introduction to SeDuMi. pages 1–24, 1998.

[76] W. Tan. *Nonlinear Control Analysis and Synthesis using Sum-of-Squares Programming*. PhD thesis, UC Berkeley, 2006.

[77] J. Z. Tang and I. R. Manchester. Transverse contraction criteria for stability of nonlinear hybrid limit cycles. *Proceedings of the IEEE Conference on Decision and Control*, (February):31–36, 2014.

[78] J. Z. Tang and I. R. Manchester. Stability and Robustness of Hybrid Nonlinear Limit Cycles for Dynamic Walking Robots. *Under Review*, 2017.

[79] J. Z. Tang, A. M. Boudali, and I. R. Manchester. Invariant Funnels for Underactuated Dynamic Walking Robots: New Phase Variable and Experimental Validation. In *IEEE International Conference on Robotics and Automation (ICRA)*, 2017.

[80] R. Tedrake, I. R. Manchester, M. Tobenkin, and J. W. Roberts. LQR-trees: Feedback Motion Planning via Sums-of-Squares Verification. *The International Journal of Robotics Research*, 29(8):1038–1052, Apr 2010.

[81] U. Topcu, A. Packard, and P. Seiler. Local stability analysis using simulations and sum-of-squares programming. *Automatica*, 44(10):2669–2675, Oct 2008.

[82] U. Topcu, A. Packard, P. Seiler, and G. Balas. Help on SOS [Ask the Experts]. *IEEE Control Systems Magazine*, 30(4):18–23, Aug 2010.

[83] P. Van den Hof. Closed-loop issues in system identification. *Annual Reviews in Control*, 22:173–186, Jan 1998.

[84] W. Wang and J. J. Slotine. On partial contraction analysis for coupled nonlinear oscillators. *Biol Cybern*, 92(1):38–53, 2005.

[85] E. Westervelt, C. Chevallereau, B. Morris, J. Grizzle, and J. Ho Choi. *Feedback Control of Dynamic Bipedal Robot Locomotion*. Automation and Control Engineering. CRC Press, Jun 2007.

[86] H. Wolkowicz, R. Saigal, and L. Vandenberghe. *Handbook of Semidefinite Programming*. 2000.

[87] X.-S. Yang. Remarks on three types of asymptotic stability. *Systems & Control Letters*, 42(4):299–302, Apr 2001.

[88] H. Ye, A. N. Michel, and L. Hou. Stability analysis of systems with impulse effects. *Automatic Control, IEEE Transactions on*, 43(12):1719–1723, 1998.

Appendix A

The Compass Gait Walker

The continuous dynamics of the compass gait walker, as shown in Fig. 4.1, can be represented in the form of Eq. (A.1),

$$M(q)\ddot{q} + C(q,\dot{q})\dot{q} + G(q) = B(q)u. \tag{A.1}$$

with $q = [\theta_{sw}, \theta_{st}]^T$, and

$$M(q) = \begin{bmatrix} M_{11} & M_{12} \\ M_{21} & M_{22} \end{bmatrix} \tag{A.2}$$

$M_{11} = ml_c^2 + I_c$
$M_{12} = M_{12} = -ml_c^2 - I_c + mll_c\cos(q_1)$
$M_{22} = 2I_c + \mathrm{m_H}l^2 + 2m(l^2 + l_c^2) - 2mll_c(1 + \cos(q_1))$

$$C(q,\dot{q}) = \begin{bmatrix} C_{11} & C_{12} \\ C_{21} & C_{22} \end{bmatrix} \tag{A.3}$$

$C_{11} = 0$
$C_{12} = -mll_c\dot{q}_2\sin(q_1)$

$C_{21} = -mll_c\,(\dot{q}_1 - \dot{q}_2)\,\sin(q_1)$
$C_{22} = mll_c\dot{q}_1\sin(q_1)$

$$G(q) = \begin{bmatrix} G_1 \\ G_2 \end{bmatrix} \tag{A.4}$$

$G_1 = \mathrm{g}_0 ml_c \sin(q_1 - q_2)$
$G_2 = -\mathrm{g}_0\,(ml_c\sin(q_1 - q_2) + (2ml - ml_c + \mathrm{m}_{\mathrm{Hg}}l)\sin(q_2))$

$$B(q) = \begin{bmatrix} 1 \\ 0 \end{bmatrix}. \tag{A.5}$$

Assuming instantaneous and rigid impact of the swing leg without rebound and slip, the impact model is defined as:

$$\Delta_q = \begin{bmatrix} -1 & 0 \\ -1 & 1 \end{bmatrix} \tag{A.6}$$

$$\Delta_{\dot{q}}(q^-) = \Delta_q[H^+(q^-)]^{-1}H^-(q^-) \tag{A.7}$$

where $H^+_{1,1}(q^-) = p_1 + p_3$
$H^+_{2,1}(q^-) = H^+_{1,2}(q^-) = p_2\cos(q_1^-) - p_1 - p_3$
$H^+_{1,1}(q^-) = -2p_2\cos(q_1^-) + p_3 + 2p_1$
$H^-_{1,1}(q^-) = p_1 - p_2;\ H^-_{2,1}(q^-) = -p_1 + p_2$
$H^-_{1,2}(q^-) = p_3\cos(q_1) - p_1 + p_2;\quad H^-_{2,2}(q^-) = p_3\cos(q_1)$
$p_1 = m\,l_c^2 + I_c;\quad p_2 = lml_c;\quad p_3 = m_H l^2 + 2ml(l - l_c)$